# Stochastic Lagrangian Dynamics of Vorticity for Viscous, Incompressible Fluids

G. L. Eyink<sup>1,2,3</sup>, A. Gupta<sup>1</sup>, and T. A. Zaki<sup>3</sup>

(Received)

Prior mathematical work of Constantin & Iyer (2008, 2011) has shown that incompressible Navier-Stokes solutions possess infinitely-many stochastic Lagrangian conservation laws for vorticity, backward in time, which generalize the invariants of Cauchy (1815) for smooth Euler solutions. We reformulate this theory for the case of wall-bounded flows by appealing to the Kuz'min (1983)-Oseledets (1989) representation of Navier-Stokes dynamics, in terms of the vortex-momentum density associated to a continuous distribution of infinitesimal vortex rings. The Constantin-Iver theory provides an exact representation for vorticity at any interior point as an average over stochastic vorticity contributions transported from the wall. We point out relations of this Lagrangian formulation with the Eulerian theory of Lighthill (1963)-Morton (1984) for vorticity generation at solid walls, and also with a statistical result of Taylor (1932)-Huggins (1994), which connects dissipative drag with organized cross-stream motion of vorticity and which is closely analogous to the "Josephson-Anderson relation" for quantum superfluids. We elaborate a Monte Carlo numerical Lagrangian scheme to calculate the stochastic Cauchy invariants and their statistics, given the Eulerian space-time velocity field. The method is validated using an online database of a turbulent channel-flow simulation (Graham et al. 2016), where conservation of the mean Cauchy invariant is verified for two selected buffer-layer events corresponding to an "ejection" and a "sweep". The variances of the stochastic Cauchy invariants grow exponentially backward in time, however, revealing Lagrangian chaos of the stochastic trajectories undergoing both fluid advection and viscous diffusion.

Key words: vortex dynamics, Navier–Stokes equations, computational methods

## 1. Introduction

Vorticity in inviscid fluids governed by incompressible Euler equations has remarkable geometric and Lagrangian properties that were derived in classic works of Cauchy (1815), Helmholtz (1858), Weber (1868), Kelvin (1868) and others. In a Hamiltonian formulation of the ideal fluid equations, these properties arise from an infinite-dimensional particle-relabelling symmetry of the action function (Salmon 1988) and they are intimately related to the modern geometric view of the Euler equations as governing geodesic flow on the space *SDiff* of volume-preserving transformations (Arnold 1966; Besse & Frisch 2017). These Lagrangian properties of vorticity have often been invoked in theories of turbulent

 $<sup>^1\</sup>mathrm{Department}$  of Applied Mathematics & Statistics, The Johns Hopkins University, Baltimore, MD 21218, USA

<sup>&</sup>lt;sup>2</sup>Department of Physics & Astronomy, The Johns Hopkins University, Baltimore, MD 21218, USA

<sup>&</sup>lt;sup>3</sup>Department of Mechanical Engineering, The Johns Hopkins University, Baltimore, MD 21218, USA

energy dissipation, especially by Taylor (1937, 1938) and Taylor & Green (1937). In these papers Taylor suggested that vortex lines which are materially advected by a turbulent flow should be lengthened by random stretching and mean-square vorticity thus enhanced by conservation of circulations. Taylor admitted, however, that vortex lines move as material lines and circulations on material loops are conserved only for ideal smooth Euler flows and these properties may be substantially modified by fluid viscosity. Subsequent works have confirmed that statistical and dynamical properties of vortex lines and material lines are quite distinct in turbulent flows. For example, Lüthi et al. (2005); Guala et al. (2005, 2006) have found in an experimental study of nearly homogeneous, isotropic turbulence that vortex stretching rates are smaller than rates of material-line stretching when both are measured along the trajectories of neutrally-buoyant polystyrene particles. A closely related numerical study of isotropic turbulence by Johnson & Meneyeau (2016) has shown that these differences in stretching rates extend even to the rare fluctuations described by large-deviations theory. Johnson et al. (2017) have furthermore shown that large-deviation statistics of vortex-stretching rates and material line-stretching rates are distinct also in turbulent channel flow. It might be inferred from these negative findings that the remarkable Lagrangian properties enjoyed by vorticity for smooth Euler flows have no relevance for physical turbulent flows, even at very high Reynolds numbers.

Recently, however, Constantin & Iyer (2008, 2011) have shown that the deep geometric and Lagrangian properties of vorticity for Euler dynamics fully extend to viscous Navier-Stokes solutions within a stochastic framework. In the setting of their theorems, a random white-noise is added to the evolution equations for Lagrangian fluid particles and this noise averaged over to represent mathematically the viscous diffusion of momentum. Constantin & Iver (2008, 2011) showed that every Navier-Stokes solution satisfies stochastic generalizations of the Weber formula (Weber 1868), the conservation of circulations (Kelvin 1868), the Cauchy formula and conserved Cauchy invariants (Cauchy 1815), with all of these results reducing in the inviscid limit to those satisfied by smooth Euler solutions. Eyink (2010) has shown that these properties follow from particle-relabelling symmetry in a stochastic least-action formulation of incompressible Navier-Stokes and Rezakhanlou (2016) has discussed the Constantin-Iver results in the setting of stochastic symplectic flows in phase-space. It should be noted that the same stochastic Lagrangian representation of vorticity as Constantin & Iyer (2008) was obtained even earlier by Rapoport (2002), section 11, as the corollary of a more general result for Navier-Stokes equations on a compact Riemannian manifold without boundary. This level of generality is not required for most applications in fluid mechanics and, unfortunately, obscures the simplicity of the results for Navier-Stokes flows in flat Euclidean space.

The established Lagrangian properties of vorticity hold both for boundary-free Navier-Stokes flows (Constantin & Iyer 2008) and for wall-bounded flows with stick b.c. on the fluid velocity (Constantin & Iyer 2011). In the latter case, however, Constantin & Iyer (2011) were able to show only existence of suitable boundary conditions in their Lagrangian formulation, without an explicit, concrete construction. We solve that problem here by exploiting the Kuz'min-Oseledets formulation of the incompressible Navier-Stokes equation in terms of the vortex-momentum density (Kuz'min 1983; Oseledets 1989). We recall that vortex momentum is the total impulse required to set a compact vortex into motion (Batchelor (2000), section 7.2) and its density can be interpreted physically as the vortex-momentum per volume when the fluid velocity field is represented by a continuous distribution of infinitesimal vortex-rings. The theory of Constantin & Iyer (2008, 2011) can be understood as a stochastic representation of viscosity in the Kuz'min-Oseledets formulation, which we show extends readily to wall-bounded flows. In this setting the Constantin & Iyer (2011) theory provides an infinite set of stochastic Cauchy invariants

for Navier-Stokes solutions, which permit an exact representation of the vorticity at any interior point in terms of vorticity at the wall. We further discuss some relations of Constantin & Iyer (2011) with the standard Eulerian theory of vorticity generation at solid boundaries due to Lighthill (1963) and Morton (1984), which relates inviscid generation of vorticity to tangential pressure gradients at the wall. Wall-bounded turbulence driven by an imposed pressure-gradient or freestream velocity differs from homogeneous, isotropic turbulence in that energy dissipation requires not just random stretching of vortex lines but in fact an organized, coherent transport of vorticity. Indeed it follows from the Lighthill-Morton theory that a mean pressure-drop down a pipe or channel implies the production of spanwise vorticity and a mean viscous flux of such vorticity away from the wall. This exact relation has been previously exploited in developing turbulent drag-control methods aimed at modifying the boundary vorticity flux (Koumoutsakos 1999; Zhao et al. 2004).

It is in fact a paradigm in the study of quantum fluids that effective drag in an otherwise non-dissipative superfluid is associated to cross-stream motion of quantized vortex lines by the so-called "Josepson-Anderson relation"; see Josephson (1962); Anderson (1966), and Packard (1998); Varoquaux (2015) for reviews. Such a result was already anticipated for classical turbulent pipe-flow by Taylor (1932) and more systematically discussed in that context by Huggins (1970, 1994) and Eyink (2008). The physical basis of the relation is very general and follows just from the local conservation of momentum, rewritten as

$$\partial_t u_i = \frac{1}{2} \epsilon_{ijk} \Sigma_{jk} - \partial_i h \tag{1.1}$$

for suitable anti-symmetric matrix  $\Sigma$  and potential h. For example, the incompressible Navier-Stokes equation when rewritten in this manner has these quantities given by

$$\Sigma_{ij} = u_i \omega_j - u_j \omega_i + \nu \left( \frac{\partial \omega_i}{\partial x_j} - \frac{\partial \omega_j}{\partial x_i} \right), \quad h = p + \frac{1}{2} |\boldsymbol{u}|^2.$$
 (1.2)

Other fluid systems will have different contributions here, e.g. a body-force  $\mathbf{f}$  from the stress of a polymer additive will contribute a term  $\Sigma_{ij} = \epsilon_{ijk} f_k$  from the Magnus effect. Taking the curl of (1.1) in general leads to the equation for local conservation of vorticity

$$\partial_t \omega_i + \partial_i \Sigma_{ij} = 0 \tag{1.3}$$

where  $\Sigma_{ij}$  gives the flux of jth component of vorticity in the ith coordinate direction. For Navier-Stokes, (1.3) is equivalent to the equation of Helmholtz (1858), with contributions to the vorticity flux in (1.2) arising from nonlinear advection, vortex-stretching and viscous diffusion, respectively. As pointed out by Taylor (1932) for 2D turbulent pipe flow and by Huggins (1994) for more general statistically steady flows, the average of (1.1) implies a pointwise relation between mean vorticity transport and the mean gradient of (generalized) pressure:

$$\overline{\Sigma}_{ij} = \epsilon_{ijk} \partial_k \overline{\left(p + \frac{1}{2} |\boldsymbol{u}|^2\right)}$$
(1.4)

with  $\partial_i \overline{\Sigma}_{ij} = 0$ . There is an inward flux of spanwise vorticity not only at the wall, as predicted by the Lighthill-Morton theory, but also in the bulk of the flow, intrinsically linked to a downstream drop in pressure or in kinetic energy density. Such vorticity flux occurs not only in pipes and channels but also in many other cases, such as turbulent free shear layers and wakes (Brown & Roshko 2012). The Constantin & Iyer (2011) theory provides a Lagrangian description of this interior vorticity transport in terms of the stochastic motion and deformation of vorticity vector elements.

The detailed contents of this paper are outlined as follows. In section 2 we present the stochastic Lagrangian formulation of Navier-Stokes, reviewing the Kuz'min-Oseledets formulation (2.1), explaining the Constantin-Iyer theory within this framework (2.2), and discussing the relation with the theories of Lighthill-Morton and Taylor-Huggins (2.3). In section 3 we present and evaluate a numerical implementation, elaborating our Monte Carlo Lagrangian scheme (3.1), describing the channel-flow database used in the study (3.2), and validating the numerical method (3.3). The conclusion section 4 discusses some open issues and prospects for future work, and an Appendix A provides some technical details on stochastic interpolation. Additional information is provided as Supplemental Materials (SM). In the following paper of Eyink et al. (2020a) (hereafter referenced as Paper II in the text) we exploit the methods of the present work to study in detail the process of vortex-lifting in the buffer-layer of turbulent channel-flow.

## 2. Stochastic Lagrangian Formulation of the Navier-Stokes Equation

The stochastic Lagrangian representation of incompressible Navier-Stokes solutions due to Constantin & Iyer (2008, 2011) was developed by them using the Weber (1868) formula. We believe that their work is better understood, however, using the closely related "vortex-momentum" formalism of Kuz'min (1983) and Oseledets (1989). Although originally derived for incompressible Euler and Navier-Stokes equations in all of Euclidean space, the Kuz'min-Oseledets formalism carries over very naturally to wall-bounded flows. We review the latter theory, first for incompressible Euler equations and then for Navier-Stokes equations at non-vanishing viscosity, both suitably generalized to flows with solid walls. Next, we explain the stochastic representations of Constantin & Iyer (2008, 2011) in this framework, simplifying in particular their own discussion of boundary conditions. As we explain, their theory yields infinitely many stochastic Lagrangian conservation laws for incompressible Navier-Stokes solutions, which generalize the vorticity invariants of Cauchy (1815) for Euler solutions. These stochastic Cauchy invariants provide a precise mathematical tool with which to trace the evolution of interior vorticity back to its origins at the solid wall. Finally, we shall briefly compare this framework with analytic theories for vorticity-generation at the flow boundary, in particular the theory of Lighthill (1963) and Morton (1984) and related work of Taylor (1932) and Huggins (1970, 1994).

## 2.1. Kuz'min-Oseledets Representation of Euler and Navier-Stokes

We begin with a few mathematical preliminaries. The Kuz'min-Oseledets theory employs essentially the Leray-Hodge projection  $\mathbb{P}$  operator on vector fields, which projects to the solenoidal component (Boyer & Fabrie (2012), section 3.3). In flow domains  $\Omega$  with a non-empty boundary  $\partial \Omega \neq \emptyset$ , this projection operator is defined on a vector field  $\mathbf{p}$  by

$$\mathbb{P}\mathbf{p} = \mathbf{p} - \nabla_x \phi, \tag{2.1}$$

where  $\phi$  is the velocity potential solving the Neumann boundary-value problem:

$$\triangle_x \phi = \nabla_x \cdot \mathbf{p}, \quad \mathbf{x} \in \Omega; \qquad \frac{\partial \phi}{\partial n} = \hat{\mathbf{n}} \cdot \mathbf{p}, \quad \mathbf{x} \in \partial \Omega.$$
 (2.2)

Here  $\hat{\boldsymbol{n}}$  is the outward-pointing unit normal vector at a point on the smooth boundary  $\partial\Omega$ . This projection yields the Hodge decomposition  $\mathbf{p} = \boldsymbol{u} + \nabla_x \phi$ , where  $\boldsymbol{u} = \mathbb{P}\mathbf{p}$  satisfies  $\nabla_x \cdot \boldsymbol{u} = 0$  on  $\Omega$  and  $\hat{\boldsymbol{n}} \cdot \boldsymbol{u} = 0$  on  $\partial\Omega$ . All of the interior vorticity of the flow arises then obviously from the solenoidal component  $\boldsymbol{u}$ . On a matter of notation, we shall use in our discussion below the convention of "dyadic products" of vectors, with  $\boldsymbol{ab}$  representing the tensor product, usually denoted by  $\boldsymbol{a} \otimes \boldsymbol{b}$  in the mathematical literature, so that

 $(ab)_{ij} = a_i b_j$ . This convention applies in particular to Jacobian derivatives  $\nabla_x a$ , so that  $(\nabla_x a)_{ij} = \partial_i a_j$ . The reader should be aware that this is different from the convention employed by Constantin & Iyer (2008, 2011), who take instead  $(\nabla_x a)_{ij} = \partial a_i/\partial x_j$ .

As observed by Kuz'min (1983), the equation

$$D_t \mathbf{p} + (\nabla_x \mathbf{u}) \mathbf{p} = \mathbf{0}, \quad \mathbf{u} = \mathbb{P} \mathbf{p}$$
 (2.3)

is equivalent to the incompressible Euler equations for u when the flow domain is all of Euclidean space. We derive a more general result below, so that here we simply observe that in unbounded space

$$\phi(\boldsymbol{x},t) = -\frac{1}{4\pi} \int d^3x' \, \frac{1}{|\boldsymbol{x} - \boldsymbol{x}'|} \boldsymbol{\nabla}_{x'} \cdot \mathbf{p}(\boldsymbol{x}',t)$$
 (2.4)

assuming good decay of  $\mathbf{p}(x',t)$  for  $|x'| \to \infty$ , and thus

$$\mathbf{u}(\mathbf{x},t) = \mathbf{p}(\mathbf{x},t) - \frac{1}{4\pi} \int d^3x' \, \frac{\mathbf{x} - \mathbf{x}'}{|\mathbf{x} - \mathbf{x}'|^3} \mathbf{\nabla}_{\mathbf{x}'} \cdot \mathbf{p}(\mathbf{x}',t). \tag{2.5}$$

Integration by parts requires care, because of the divergence at x' = x. Removing a small ball  $|x' - x| < \epsilon$  in the x'-integral and taking the limit  $\epsilon \to 0$  gives

$$\mathbf{u}(\mathbf{x},t) = \frac{2}{3}\mathbf{p}(\mathbf{x},t) + \int d^3x' \ \mathbf{G}(\mathbf{x} - \mathbf{x}')\mathbf{p}(\mathbf{x}',t), \quad G_{ij}(\mathbf{r}) = \frac{1}{4\pi} \left( \frac{3r_i r_j}{r^5} - \frac{\delta_{ij}}{r^3} \right). \quad (2.6)$$

where the second term is a principal-value integral with respect to the singular kernel. As is well-known (Batchelor (2000), section 7.2),  $\mathbf{u}_0(\mathbf{x}) = \frac{2}{3} \mathbf{P} \, \delta^3(\mathbf{x} - \mathbf{x}_0) + \mathbf{G}(\mathbf{x} - \mathbf{x}_0) \mathbf{P}$  is the velocity field of a vortex ring with impulse  $\mathbf{P} = (1/2) \int d^3x \ \mathbf{x} \times \boldsymbol{\omega}(\mathbf{x}, t)$  which is centered at  $\mathbf{x}_0$  and whose radius is taken to vanish with  $\mathbf{P}$  fixed. The first delta-function term in the velocity  $\mathbf{u}_0$  is necessary to enforce incompressibility but vanishes for  $\mathbf{x} \neq \mathbf{x}_0$ . Both Kuz'min (1983) and Oseledets (1989) therefore interpreted  $\mathbf{p}(\mathbf{x}, t)$  physically as the "vortex-momentum density" resulting from a distribution  $\sum_{n=1}^{N} \mathbf{P}_n(t) \delta^3(\mathbf{x} - \mathbf{X}_n(t))$  of infinitesimal vortex-rings in the limit as  $N \to \infty$ . For finite N, variables  $\mathbf{X}_n(t)$ ,  $\mathbf{P}_n(t)$ , n = 1, ..., N obey Hamiltonian equations of motion derived by Roberts (1972).

Generalizing the result of Kuz'min (1983), we now show that the equivalence of the Kuz'min-Oseledets equation (2.3) with Euler extends to wall-bounded flows, where boundary conditions  $\hat{\mathbf{n}} \cdot \mathbf{p} = \partial \phi / \partial n$  on  $\mathbf{p}$  imply the standard conditions of no-flow through the boundary on velocity  $\mathbf{u}$ . Indeed, direct substitution of  $\mathbf{p} = \mathbf{u} + \nabla_x \phi$  into (2.3) gives

$$D_t \boldsymbol{u} + \boldsymbol{\nabla}_x \left( D_t \phi + \frac{1}{2} |\boldsymbol{u}|^2 \right) = \boldsymbol{0}. \tag{2.7}$$

Defining pressure p up to a space-independent constant c(t) by

$$D_t \phi + \frac{1}{2} |\mathbf{u}|^2 - p = c(t)$$
 (2.8)

then gives

$$D_t \boldsymbol{u} = -\boldsymbol{\nabla}_x \boldsymbol{p} \tag{2.9}$$

which has the form of the incompressible Euler equations with kinematic pressure p. The constraint of incompressibility  $\nabla_x \cdot \boldsymbol{u} = 0$  implies the standard Poisson equation

$$-\triangle_x p = \operatorname{Tr}((\boldsymbol{\nabla}_x \boldsymbol{u})^\top (\boldsymbol{\nabla}_x \boldsymbol{u})). \tag{2.10}$$

Furthermore, applying  $\partial/\partial n$  to the Eq.(2.8) defining p and using  $\partial\phi/\partial n = \hat{\mathbf{n}} \cdot \mathbf{p}$  gives

$$\frac{\partial p}{\partial n}\Big|_{\partial\Omega} = \nabla_x \hat{\boldsymbol{n}} : \boldsymbol{u}\boldsymbol{u} + \hat{\boldsymbol{n}} \cdot [D_t \mathbf{p} + (\nabla_x \boldsymbol{u})\mathbf{p}]. \tag{2.11}$$

Together with Eq.(2.3) for  $\mathbf{p}$ , this yields

$$\left. \frac{\partial p}{\partial n} \right|_{\partial \Omega} = \nabla_x \hat{\boldsymbol{n}} : \boldsymbol{u}\boldsymbol{u}, \tag{2.12}$$

which are the standard pressure b.c. for incompressible Euler arising from the condition of no-flow through the boundary. In order to impose initial conditions  $\mathbf{u}(t=t_0)=\mathbf{u}_0$  for a suitable choice of  $\mathbf{u}_0$ , satisfying  $\nabla_x \cdot \mathbf{u}_0 = 0$  and  $\hat{\mathbf{n}} \cdot \mathbf{u}_0|_{\partial\Omega} = 0$ , one may make an arbitrary choice of  $\phi_0$  and take  $\mathbf{p}_0 = \mathbf{u}_0 + \nabla_x \phi_0$  as initial data for (2.3). In that case, the equation (2.8) for  $\phi$  must be solved with the initial condition

$$\phi(t = t_0) = \phi_0. \tag{2.13}$$

Remarkably, initial and boundary conditions for the first-order, hyperbolic PDE (2.8) are unconstrained except by the requirement of a solution smooth up to the boundary. Physically, one may interpret different choices of  $\phi$  that solve this equation to correspond to different sets of image vortices outside  $\Omega$  that are needed to produce a net incompressible velocity  $\boldsymbol{u}$  with zero flow though the boundary, for different momentum distributions  $\mathbf{p}$  of vortex-rings inside  $\Omega$ . In this way the initial-boundary value problem of the Kuz'min-Oseledets equation is equivalent to the initial-boundary-value problem of incompressible Euler, except that there are infinitely many distinct choices of  $\mathbf{p}$ ,  $\phi$  that correspond to the same  $\boldsymbol{u}$ , p.

Using the vector calculus identity  $\mathbf{u} \times (\nabla_x \times \mathbf{p}) = (\nabla_x \mathbf{p})\mathbf{u} - (\mathbf{u} \cdot \nabla_x)\mathbf{p}$ , the Kuz'min-Oseledets equation can be rewritten as

$$\partial_t \mathbf{p} = \mathbf{u} \times (\nabla_x \times \mathbf{p}) - \nabla_x (\mathbf{p} \cdot \mathbf{u}). \tag{2.14}$$

Because  $\mathbf{p}$  and  $\mathbf{u}$  differ only by a gradient, they have same curl:

$$\nabla_x \times \mathbf{p} = \nabla_x \times \mathbf{u} := \omega. \tag{2.15}$$

Taking the curl of Eq.(2.3) rewritten as (2.14) then obviously yields the standard inviscid Helmholtz equation for the vorticity:

$$\partial_t \boldsymbol{\omega} = \boldsymbol{\nabla}_x \times (\boldsymbol{u} \times \boldsymbol{\omega}). \tag{2.16}$$

Yet another form of Eq.(2.3) follows by regarding  $p_i$  as the components of a differential 1-form  $p_i dx^i$ , in which case the equation becomes (Oseledets 1989)

$$\partial_t \mathbf{p} + \mathcal{L}_{\boldsymbol{u}} \mathbf{p} = \mathbf{0}, \tag{2.17}$$

for the *Lie-derivative* on 1-forms defined by

$$\mathcal{L}_{\boldsymbol{u}}\mathbf{p} := (\boldsymbol{u} \cdot \boldsymbol{\nabla}_{x})\mathbf{p} + (\boldsymbol{\nabla}_{x}\boldsymbol{u})\mathbf{p}. \tag{2.18}$$

See Tur & Yanovsky (1993); Besse & Frisch (2017) for introductions to this concept from differential geometry generalizing the standard material derivative. The form (2.17) of the Kuz'min-Oseledets equation makes manifest its remarkable geometric and Lagrangian properties. In fact, as a Lie-transported 1-form, vortex-momentum  $\mathbf{p}$  can be represented in terms of its initial data  $\mathbf{p}_0$  by the Lagrangian "back-to-labels" map  $\mathbf{A}(\mathbf{x},t)$  as

$$\mathbf{p}(\boldsymbol{x},t) = (\boldsymbol{\nabla}_{x}\boldsymbol{A}) \cdot \mathbf{p}_{0}(\boldsymbol{A}(\boldsymbol{x},t)). \tag{2.19}$$

As usual, the map  $\mathbf{A}(\mathbf{x},t)$  is defined to have zero material-derivative  $D_t \mathbf{A} = \mathbf{0}$  and satisfies  $\mathbf{A}(\mathbf{x},t_0) = \mathbf{x}$  at the labelling time  $t_0$ . Result (2.19) can be interpreted as the "push-forward" of the differential 1-form under the Lagrangian flow (Besse & Frisch 2017) and can be verified in a pedestrian manner using the matrix differential equation

$$D_t(\nabla_x A) + (\nabla_x u)(\nabla_x A) = \mathbf{O}$$
(2.20)

which follows by taking the gradient of  $D_t \mathbf{A} = \mathbf{0}$ . By taking a curl of (2.19), one immediately obtains the famous Cauchy formula (Cauchy, 1815) for the vorticity

$$\boldsymbol{\omega}(\boldsymbol{x},t) = (\boldsymbol{\nabla}_{\boldsymbol{x}}\boldsymbol{A})^{\top - 1}\boldsymbol{\omega}_0(\boldsymbol{A}(\boldsymbol{x},t)) = (\boldsymbol{\omega}_0(\boldsymbol{a}) \cdot \boldsymbol{\nabla}_{\boldsymbol{a}})\boldsymbol{X}|_{\boldsymbol{X}(\boldsymbol{a},t) = \boldsymbol{x}}, \quad (2.21)$$

where X(a,t) is the standard Lagrangian flow map that satisfies

$$(d/dt)X(\boldsymbol{a},t) = \boldsymbol{u}(X(\boldsymbol{a},t),t), \quad X(\boldsymbol{a},t_0) = \boldsymbol{a}$$
(2.22)

and which is the inverse map to A(x,t). To obtain the first equality in (2.21) we used the simple identity  $\epsilon_{ijk} \frac{\partial A_l}{\partial x_i} \frac{\partial A_m}{\partial x_j} \frac{\partial A_n}{\partial x_k} = \epsilon_{lmn}$  for an incompressible flow. The Cauchy formula can be regarded also as a "push-forward" of the vorticity as a differential 2-form (Besse & Frisch 2017). This result succinctly expresses the "frozen-in" property of vorticity for smooth Euler solutions. In particular, the inverse formula to (2.21)

$$\boldsymbol{\omega}_0(\boldsymbol{a}) = (\boldsymbol{\nabla}_a \boldsymbol{X})^{\top - 1} \boldsymbol{\omega}(\boldsymbol{X}(\boldsymbol{a}, t), t) = (\boldsymbol{\omega}(\boldsymbol{x}, t) \cdot \boldsymbol{\nabla}_x) \boldsymbol{A}(\boldsymbol{x}, t)|_{\boldsymbol{A}(\boldsymbol{x}, t) = \boldsymbol{a}}$$
(2.23)

defines the Cauchy invariants, which are independent of time t for every choice of particle label a, thus comprising an infinite set of Lagrangian conserved quantities for Euler (Frisch & Villone 2014). It is intriguing to note, incidentally, that the hyperbolic equation (2.8) for the velocity potential  $\phi$  can also be solved in terms of Lagrangian flows (method of characteristics) and when  $c(t) \equiv 0$  one finds

$$\phi(\mathbf{X}(\mathbf{a},t),t) = \phi(\mathbf{a},t_0) - \int_{t_0}^t ds \left[ \frac{1}{2} |\dot{\mathbf{X}}(\mathbf{a},s)|^2 - p(\mathbf{X}(\mathbf{a},s),s) \right]. \tag{2.24}$$

Hence, this potential is directly related to the (negative of) the *action*, which is locally minimized by particle trajectories for incompressible Euler solutions (Brenier 2003).

It was noted in passing by Kuz'min (1983) and developed in more detail by Oseledets (1989) that a similar equivalence holds between the equation

$$D_t \mathbf{p} + (\nabla_x \mathbf{u}) \mathbf{p} = \nu \triangle_x \mathbf{p}, \quad \mathbf{u} = \mathbb{P} \mathbf{p}$$
 (2.25)

and the incompressible Navier-Stokes equation for  $\boldsymbol{u}$ , at least for flows in unbounded, Euclidean space. This equivalence extends to wall-bounded flows in any spatial domain  $\Omega$ , with stick b.c. on velocity  $\boldsymbol{u}$  corresponding to the condition  $\mathbf{p} = \nabla_x \phi$  at  $\partial \Omega$ . More generally, one may consider walls moving with tangential velocity  $\boldsymbol{u}_W$  so that  $\hat{\boldsymbol{n}} \cdot \boldsymbol{u}_W = 0$ , where the Leray-Hodge decomposition remains defined as in Eqs.(2.1),(2.2). The stick b.c.  $\boldsymbol{u} = \boldsymbol{u}_W$  then correspond to the condition  $\mathbf{p} = \boldsymbol{u}_W + \nabla_x \phi$  at  $\partial \Omega$ . Indeed, as for Euler, direct substitution of  $\mathbf{p} = \boldsymbol{u} + \nabla_x \phi$  into (2.25) gives

$$D_t \boldsymbol{u} + \boldsymbol{\nabla}_x \left( D_t \phi + \frac{1}{2} |\boldsymbol{u}|^2 - \nu \triangle_x \phi \right) = \nu \triangle_x \boldsymbol{u}. \tag{2.26}$$

Defining pressure p up to a space-independent constant c(t) by

$$D_t \phi - \nu \triangle_x \phi + \frac{1}{2} |\mathbf{u}|^2 - p = c(t)$$
(2.27)

then gives

$$D_t \boldsymbol{u} = -\boldsymbol{\nabla}_x p + \nu \triangle_x \boldsymbol{u} \tag{2.28}$$

which has the form of the incompressible Navier-Stokes equations. The constraint of incompressibility implies the standard Poisson equation for the pressure p, just as for Euler. Similarly, applying  $\partial/\partial n$  to Eq.(2.27) defining p and using  $\partial\phi/\partial n = \hat{\mathbf{n}} \cdot \mathbf{p}$ ,

$$\frac{\partial p}{\partial n}\Big|_{\partial\Omega} = \nabla_x \hat{\boldsymbol{n}} : \boldsymbol{u}_W \boldsymbol{u}_W + \hat{\boldsymbol{n}} \cdot \nu \triangle_x \boldsymbol{u} + \hat{\boldsymbol{n}} \cdot [D_t \mathbf{p} - \nu \triangle_x \mathbf{p} + (\nabla_x \boldsymbol{u}) \mathbf{p}]. \tag{2.29}$$

Together with the viscous Kuz'min-Oseledets equation (2.25) for p, this yields

$$\left. \frac{\partial p}{\partial n} \right|_{\partial \Omega} = \nabla_x \hat{\boldsymbol{n}} : \boldsymbol{u}_W \boldsymbol{u}_W + \hat{\boldsymbol{n}} \cdot \nu \triangle_x \boldsymbol{u}, \tag{2.30}$$

which are the standard pressure b.c. for incompressible Navier-Stokes. Just as for Euler, any solenoidal initial condition  $\mathbf{u}(t=t_0)=\mathbf{u}_0$  for Navier-Stokes can be obtained by solving the Kuzmin-Oseledets equation (2.25) with the corresponding initial condition  $\mathbf{p}(t=t_0)=\mathbf{p}_0:=\mathbf{u}_0+\nabla_x\phi_0$  for any choice of  $\phi_0$ . In that case, the parabolic linear equation (2.27) must be solved with initial condition  $\phi(t=t_0)=\phi_0$  but with any choice of boundary conditions  $\phi=\phi_W$  on  $\partial\Omega$  (and any choice of the constant c(t)). In that case,  $\mathbf{p}=\mathbf{u}+\nabla_x\phi$  will give the corresponding solution of (2.25) with the boundary condition  $\mathbf{p}=\mathbf{u}_W+\nabla_x\phi$  on  $\partial\Omega$ . Just as for the inviscid case, the initial-boundary value problem of the viscous Kuz'min-Oseledets equation (2.25) is equivalent to the initial-boundary-value problem of the incompressible Navier-Stokes equation, but with infinitely many distinct choices of  $\mathbf{p}$ ,  $\phi$  corresponding to the same  $\mathbf{u}$ , p.

Using the vector calculus identity  $\nabla_x \times (\nabla_x \times \mathbf{p}) = \nabla_x (\nabla_x \cdot \mathbf{p}) - \triangle \mathbf{p}$ , the viscous Kuz'min-Oseledets equation (2.25) can be rewritten in the same manner as the inviscid equation:

$$\partial_t \mathbf{p} + \nabla_x (\mathbf{p} \cdot \mathbf{u} - \nu \nabla_x \cdot \mathbf{p}) = \mathbf{u} \times (\nabla_x \times \mathbf{p}) - \nu \nabla_x \times (\nabla_x \times \mathbf{p}). \tag{2.31}$$

Since it remains true that  $\mathbf{p}$  and  $\mathbf{u}$  have the same curl, taking the curl of (2.31) immediately yields the viscous Helmholtz equation for the vorticity

$$\partial_t \boldsymbol{\omega} = \boldsymbol{\nabla}_x \times (\boldsymbol{u} \times \boldsymbol{\omega}) + \nu \Delta_x \boldsymbol{\omega}, \tag{2.32}$$

which, of course, follows also from the Navier-Stokes equation. Unlike for Euler equations, however, it has not been so obvious when viscosity is non-vanishing how to exploit the Kuz'min-Oseledets formulation in order to obtain simple geometric and Lagrangian properties of vorticity. Constantin & Iyer (2008, 2011) have achieved this by exploiting a mathematical representation of viscosity in the Lagrangian framework via stochastic Brownian motion, as we now briefly explain.

#### 2.2. Constantin-Iyer Stochastic Lagrangian Formulation

As has been noted many places in the mathematics (Freidlin (1985), Oksendal (2013)), physics (Shraiman & Siggia (1994), Falkovich et al. (2001)) and engineering (Sawford (2001), Keanini (2006)) literatures, Laplacian diffusion can be represented in a Lagrangian formulation by a suitable Brownian motion. For diffusion of momentum by kinematic viscosity  $\nu$ , this involves stochastic Lagrangian trajectories that, backward in time, may be regarded as generalizations of the deterministic "back-to-labels" map. Precisely,  $\tilde{A}_t^s(x) = (\tilde{a}_t^s(x), \tilde{b}_t^s(x), \tilde{c}_t^s(x))$  for  $x \in \Omega$  is defined to satisfy

$$\widehat{d}\widetilde{\boldsymbol{A}}_{t}^{s}(\boldsymbol{x}) = \boldsymbol{u}(\widetilde{\boldsymbol{A}}_{t}^{s}(\boldsymbol{x}), s) ds + \sqrt{2\nu} \, \widehat{d}\widetilde{\boldsymbol{W}}(s), \quad s < t; \qquad \widetilde{\boldsymbol{A}}_{t}^{t}(\boldsymbol{x}) = \boldsymbol{x}$$
 (2.33)

Here the notation " $\hat{\mathbf{d}}$ " with a hat denotes the backward Itō differential, which is exactly the time-reverse of the standard (forward) Itō differential, and  $\widetilde{\mathbf{W}}(s)$  is a vector Brownian motion/stochastic Wiener process. Since the backward Itō calculus is less well-known than the forward calculus, we refer readers to the mathematical monographs of Friedman (2006) and Kunita (1997) which develop the subject at length. Setting  $\nu=0$ , one recovers a deterministic ODE, whose solution  $\boldsymbol{A}_t^s(\boldsymbol{x})$  is the usual "back-to-label" map, for labelling time s. Thus,  $\boldsymbol{A}_t^0(\boldsymbol{x}) = \boldsymbol{A}(\boldsymbol{x},t)$  in the notations of the previous section. Note, however, that the random process  $\boldsymbol{\tilde{A}}_t^s(\boldsymbol{x})$  is not guaranteed to attain time s=0 before exiting

from the domain. For any point  $\boldsymbol{x} \in \Omega$ , the stochastic particle trajectory  $\widetilde{\boldsymbol{A}}_t^s(\boldsymbol{x})$  released at time t first hits the boundary  $\partial\Omega$  at some finite, random time  $s = \tilde{\sigma}_t(\boldsymbol{x}) < t$ , evolving backward. The stochastic Lagrangian representations obtained by Constantin & Iyer (2011) for wall-bounded flows involve the "stopped process"  $\widetilde{\boldsymbol{A}}_t^{s'}(\boldsymbol{x}) := \widetilde{\boldsymbol{A}}_t^{s\vee\tilde{\sigma}_t(\boldsymbol{x})}(\boldsymbol{x})$ , which halts the stochastic Lagrangian particle as soon as it first hits the boundary, with the mathematical notation  $s \vee \tilde{\sigma}_t(\boldsymbol{x}) := \max\{s, \tilde{\sigma}_t(\boldsymbol{x})\}$ . Since the realizations of  $\tilde{\sigma}_t(\boldsymbol{x})$  are almost surely non-differentiable in  $\boldsymbol{x}$ , we always take  $\nabla_x \widetilde{\boldsymbol{A}}_t^{s'}(\boldsymbol{x}) := \nabla_x \widetilde{\boldsymbol{A}}_t^{\sigma}(\boldsymbol{x}) \Big|_{\sigma = s \vee \tilde{\sigma}_t(\boldsymbol{x})}$  below.

With these notations, Constantin & Iyer (2011) in their Lemma 5.1 obtained the following stochastic Lagrangian representation of vortex momentum  $\mathbf{p}$  solving the viscous Kuz'min-Oseledets equation, with  $\mathbb{E}$  denoting average over the random Brownian motions:

$$\mathbf{p}(\boldsymbol{x},t) = \mathbb{E}\left[\boldsymbol{\nabla}_{x}\widetilde{\boldsymbol{A}}_{t}^{0\prime}(\boldsymbol{x}) \cdot \mathbf{p}_{dat}\left(\widetilde{\boldsymbol{A}}_{t}^{0\prime}(\boldsymbol{x}), 0 \vee \widetilde{\sigma}_{t}(\boldsymbol{x})\right)\right]. \tag{2.34}$$

Here  $\mathbf{p}_{dat}$  represents the initial-boundary data, with  $\mathbf{p}_{dat}(\boldsymbol{x},t) = \mathbf{p}_0(\boldsymbol{x})$  for t=0 and  $\mathbf{p}_{dat}(\boldsymbol{x},t) = \mathbf{p}_W(\boldsymbol{x},t)$  for  $\boldsymbol{x} \in \partial \Omega$ . Using the results of the previous subsection, the stochastic representation of the Navier-Stokes velocity stated in Theorem 3.1 of Constantin & Iyer (2011) follows as a simple corollary:

$$u(\boldsymbol{x},t) = \mathbb{PE}\left[\boldsymbol{\nabla}_{x}\widetilde{\boldsymbol{A}}_{t}^{0\prime}(\boldsymbol{x}) \cdot \mathbf{p}_{dat}\left(\widetilde{\boldsymbol{A}}_{t}^{0\prime}(\boldsymbol{x}), 0 \vee \tilde{\sigma}_{t}(\boldsymbol{x})\right)\right]$$
$$= \mathbb{E}\left[\boldsymbol{\nabla}_{x}\widetilde{\boldsymbol{A}}_{t}^{0\prime}(\boldsymbol{x}) \cdot \mathbf{p}_{dat}\left(\widetilde{\boldsymbol{A}}_{t}^{0\prime}(\boldsymbol{x}), 0 \vee \tilde{\sigma}_{t}(\boldsymbol{x})\right)\right] - \boldsymbol{\nabla}\phi(\boldsymbol{x},t)$$
(2.35)

with  $\mathbf{p}_0 = \mathbf{u}_0 + \nabla_x \phi_0$  at t = 0 for any choice of  $\phi_0$  and with  $\mathbf{p}_W = \mathbf{u}_W + \nabla \phi$  at  $\partial \Omega$ , where  $\phi$  solves equation (2.27) for initial data  $\phi_0$  and an arbitrary choice of b.c.  $\phi_W$  on  $\partial \Omega$ . Constantin & Iyer (2011) used as initial data  $\mathbf{p}_0 = \mathbf{u}_0$  only and also gave only an existence argument for suitable boundary data  $\mathbf{p}_W$ , but our use of the Kuz'min-Oseledets formalism provides a complete and explicit representation for the possible data. An interesting point is that this representation implies directly that  $\hat{\mathbf{n}} \cdot \boldsymbol{\omega}|_{\partial \Omega} = 0$  for motionless walls, since on the boundary  $\hat{\mathbf{n}} \cdot \boldsymbol{\omega} = (\hat{\mathbf{n}} \times \nabla_x) \cdot \mathbf{p}_W = (\hat{\mathbf{n}} \times \nabla_x) \cdot \nabla_x \phi = 0$ . Constantin & Iyer (2011) provided also in their Proposition 6.1 a stochastic Lagrangian representation of Navier-Stokes vorticity:

$$\boldsymbol{\omega}(\boldsymbol{x},t) = \mathbb{E}\left[ (\boldsymbol{\nabla}_{x} \widetilde{\boldsymbol{A}}_{t}^{0\prime}(\boldsymbol{x}))^{\top - 1} \cdot \boldsymbol{\omega}_{dat} \left( \widetilde{\boldsymbol{A}}_{t}^{0\prime}(\boldsymbol{x}), 0 \vee \tilde{\sigma}_{t}(\boldsymbol{x}) \right) \right], \tag{2.36}$$

with likewise  $\omega_{dat}(\boldsymbol{x},t) = \omega_0(\boldsymbol{x})$  for t=0 and  $\omega_{dat}(\boldsymbol{x},t) = \omega_W(\boldsymbol{x},t)$  for  $\boldsymbol{x} \in \partial \Omega$ . The boundary data  $\omega_W$  for the Navier-Stokes vorticity is not provided directly, of course, but only indirectly and non-locally by the stick b.c.  $\boldsymbol{u} = \boldsymbol{u}_W$  on the velocity field. In both of the formulas (2.34) and (2.36), the solutions are represented by ensemble averages involving the initial and boundary data. However, in a flow entirely bounded by walls and asymptotically for very large t the event  $\tilde{\sigma}_t(\boldsymbol{x}) > 0$  holds with overwhelming probability, so that the solutions then depend almost entirely on the boundary data and almost not at all on the initial data.

We refer to the paper of Constantin & Iyer (2011) for detailed proofs of their Lemma 5.1 and Proposition 6.1. Here we give only very briefly the main idea of the argument. To prove Lemma 5.1, one obtains an evolution equation in s for  $\nabla_x \tilde{\boldsymbol{A}}_t^s(\boldsymbol{x}) \cdot \mathbf{p} \left( \tilde{\boldsymbol{A}}_t^s(\boldsymbol{x}), s \right)$  with  $\mathbf{p}$  a given solution of the viscous Kuz'min-Oseledets equation (2.25), starting at s = t and integrating backward to  $s = 0 \vee \tilde{\sigma}_t(\boldsymbol{x})$ . By taking the gradient of the stochastic

10

ODE (2.33) for particle trajectories, one obtains

$$d(\boldsymbol{\nabla}_{x}\widetilde{\boldsymbol{A}}_{t}^{s}) = (\boldsymbol{\nabla}_{x}\widetilde{\boldsymbol{A}}_{t}^{s})(\boldsymbol{\nabla}_{x}\boldsymbol{u})\Big|_{(\widetilde{\boldsymbol{A}}_{t}^{s},s)}ds, \quad s < t; \qquad \boldsymbol{\nabla}_{x}\widetilde{\boldsymbol{A}}_{t}^{t} = \mathbf{I}$$
(2.37)

which is now a deterministic ODE (along a stochastic trajectory) because the gradient of the Brownian motion vanishes. This ODE for the component column vectors  $\nabla_x \tilde{a}_t^s(x)$ ,  $\nabla_x \tilde{b}_t^s(x)$ ,  $\nabla_x \tilde{c}_t^s(x)$  of  $\nabla_x \tilde{A}_t^s$  closely resembles that describing Lie-transport of a contravariant vector, except that it describes evolution along a stochastic trajectory  $(\tilde{A}_t^s, s)$  backward in time s < t. On the other hand, using the backward Itō lemma and the fact that  $\mathbf{p}$  solves the viscous Kuz'min-Oseledets equation (2.25) gives

$$\hat{\mathbf{d}}\mathbf{p}\left(\widetilde{\boldsymbol{A}}_{t}^{s},s\right) = \left[D_{s}\mathbf{p} - \nu \triangle_{x}\mathbf{p}\right]\Big|_{(\widetilde{\boldsymbol{A}}_{t}^{s},s)} ds + \sqrt{2\nu} \,\hat{\mathbf{d}}\widetilde{\mathbf{W}}(s) \cdot \boldsymbol{\nabla})\mathbf{p}\Big|_{(\widetilde{\boldsymbol{A}}_{t}^{s},s)}, \quad t > s > 0 \vee \tilde{\sigma}_{t}(\boldsymbol{x})$$

$$= -(\boldsymbol{\nabla}_{x}\boldsymbol{u})\mathbf{p}\Big|_{(\widetilde{\boldsymbol{A}}_{t}^{s},s)} ds + \sqrt{2\nu} \,\hat{\mathbf{d}}\widetilde{\mathbf{W}}(s) \cdot \boldsymbol{\nabla})\mathbf{p}\Big|_{(\widetilde{\boldsymbol{A}}_{t}^{s},s)}. \tag{2.38}$$

Note that the backward Itō lemma supplies the viscous diffusion term  $-\nu \triangle_x \mathbf{p}$  with the correct negative sign, whereas the more familiar forward Itō stochastic flow would yield instead  $+\nu \triangle_x \mathbf{p}$  with a positive sign. Equation (2.38) resembles that describing the Lietransport of a 1-form (covariant vector) but contains an additional random term from the Brownian motion. Combining (2.37) and (2.38) then leads to the final result:

$$\hat{\mathbf{d}}\left[\boldsymbol{\nabla}_{x}\widetilde{\boldsymbol{A}}_{t}^{s}\cdot\mathbf{p}\left(\widetilde{\boldsymbol{A}}_{t}^{s},s\right)\right] = \sqrt{2\nu}\left(\boldsymbol{\nabla}_{x}\widetilde{\boldsymbol{A}}_{t}^{s}\right)\left(\hat{\mathbf{d}}\widetilde{\mathbf{W}}(s)\cdot\boldsymbol{\nabla}\right)\mathbf{p}\Big|_{\left(\widetilde{\boldsymbol{A}}_{t}^{s},s\right)} \quad t>s>0 \ \forall \ \tilde{\sigma}_{t}(\boldsymbol{x}) \quad (2.39)$$

This yields the representation of Lemma 5.1, because the final surviving term on the righthand side is a backward martingale with zero average. In fact, we obtain the even stronger result that  $\nabla_x \tilde{\boldsymbol{A}}_t^s(\boldsymbol{x}) \cdot \mathbf{p} \left( \tilde{\boldsymbol{A}}_t^s(\boldsymbol{x}), s \right)$  is a backward martingale, which is thus stochastically conserved and whose (deterministic) value  $\mathbf{p}(\boldsymbol{x},t)$  at s=t is equal to its average value at  $s=0 \vee \tilde{\sigma}_t(\boldsymbol{x})$ .

In the same manner for any solution  $\omega$  of the viscous Helmholtz equation (2.32) one has the backward martingale evolving as:

$$\hat{\mathbf{d}}\left[ (\boldsymbol{\nabla}_{x} \widetilde{\boldsymbol{A}}_{t}^{s})^{\top - 1} \cdot \boldsymbol{\omega} \left( \widetilde{\boldsymbol{A}}_{t}^{s}, s \right) \right] = \sqrt{2\nu} \left( \boldsymbol{\nabla}_{x} \widetilde{\boldsymbol{A}}_{t}^{s} \right)^{\top - 1} \left( \hat{\mathbf{d}} \widetilde{\mathbf{W}}(s) \cdot \boldsymbol{\nabla} \right) \boldsymbol{\omega} \Big|_{(\widetilde{\boldsymbol{A}}_{t}^{s}, s)} \quad t > s > 0 \lor \widetilde{\sigma}_{t}(\boldsymbol{x})$$

$$(2.40)$$

and this yields the representation for vorticity in Proposition 6.1. The derivation of (2.40) is very similar to that given for (2.39). First, it follows immediately from (2.37) that

$$d(\boldsymbol{\nabla}_{x}\widetilde{\boldsymbol{A}}_{t}^{s}(\boldsymbol{x}))^{-1\top} = -(\boldsymbol{\nabla}_{x}\widetilde{\boldsymbol{A}}_{t}^{s}(\boldsymbol{x}))^{-1\top} \cdot (\boldsymbol{\nabla}_{x}\boldsymbol{u})^{\top} \Big|_{(\widetilde{\boldsymbol{A}}_{t}^{s},s)} ds, \quad s < t; \qquad (\boldsymbol{\nabla}_{x}\widetilde{\boldsymbol{A}}_{t}^{t}(\boldsymbol{x}))^{-1\top} = \mathbf{I}$$
(2.41)

Component row vectors of  $(\nabla_x \widetilde{\boldsymbol{A}}_t^s(\boldsymbol{x}))^{-1\top}$  represent  $(\nabla_a \widetilde{\boldsymbol{x}}_t^s(\boldsymbol{a}))^{\top}$ ,  $(\nabla_a \widetilde{\boldsymbol{y}}_t^s(\boldsymbol{a}))^{\top}$ ,  $(\nabla_a \widetilde{\boldsymbol{x}}_t^s(\boldsymbol{a}))^{\top}$  and equation (2.41) describes their quasi-Lie-transport as 1-forms (covariant derivatives). On the other hand, from the backward Itō lemma and the Helmholtz equation

$$\hat{\mathbf{d}}\boldsymbol{\omega}\left(\widetilde{\boldsymbol{A}}_{t}^{s},s\right) = \left[D_{s}\boldsymbol{\omega} - \nu \triangle_{x}\boldsymbol{\omega}\right]\Big|_{(\widetilde{\boldsymbol{A}}_{t}^{s},s)} \mathbf{d}s + \sqrt{2\nu} \left(\hat{\mathbf{d}}\widetilde{\mathbf{W}}(s) \cdot \boldsymbol{\nabla}\right)\boldsymbol{\omega}\Big|_{(\widetilde{\boldsymbol{A}}_{t}^{s},s)}$$

$$= (\boldsymbol{\omega} \cdot \boldsymbol{\nabla}_{x})\boldsymbol{u}\Big|_{(\widetilde{\boldsymbol{A}}_{t}^{s},s)} \mathbf{d}s + \sqrt{2\nu} \left(\hat{\mathbf{d}}\widetilde{\mathbf{W}}(s) \cdot \boldsymbol{\nabla}\right)\boldsymbol{\omega}\Big|_{(\widetilde{\boldsymbol{A}}_{t}^{s},s)}$$

$$t > s > 0 \lor \widetilde{\sigma}_{t}(\boldsymbol{x})$$

Except for the new stochastic term from the Brownian motion, this equation describes quasi-Lie-transport of the vorticity as a covariant vector (the Hodge dual of the vorticity 2-form  $(\partial_i u_j - \partial_j u_i) dx^i dx^j$ ). Combining (2.41), (2.42) yields the result (2.40).

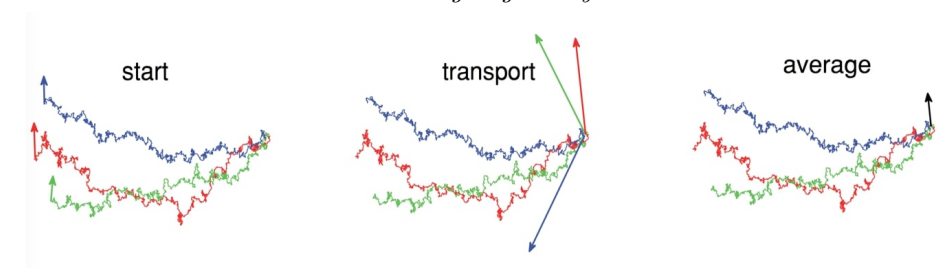


Figure 1: Illustration of the stochastic representation, with three sample realizations shown in blue, red, and green. Left: Input vectors at time  $\tau = 0 \vee \tilde{\sigma}_t(\boldsymbol{x})$  are sampled at random locations by stochastic Lagrangian trajectories going backward in time  $\tau$  from space-time point  $(\boldsymbol{x},t)$ . Middle: The vectors are Lie-transported along the stochastic trajectories forward in time from  $\tau = 0 \vee \tilde{\sigma}_t(\boldsymbol{x})$  to  $\tau = t$ , when the vectors arrive to point  $\boldsymbol{x}$  stretched and rotated by the flow. Right: The random vectors at  $(\boldsymbol{x},t)$  are ensemble-averaged to obtain the resultant vector.

The intuitive meaning of these formulas becomes more clear if one integrates along stochastic trajectories  $\widetilde{\boldsymbol{A}}_t^{\tau}(\boldsymbol{x})$  forward in time from  $\tau = 0 \vee \widetilde{\sigma}_t(\boldsymbol{x})$  to  $\tau = t$ , rather than backward in time. Note that an explicit solution for  $\nabla_x \widetilde{\boldsymbol{A}}_t^s$  is given by the time-ordered matrix exponential, with matrix products ordered right to left for increasing time:

$$\nabla_x \widetilde{\boldsymbol{A}}_t^s = \text{Texp}\left[-\int_s^t dr \ (\boldsymbol{\nabla}_x \boldsymbol{u})|_{(\widetilde{\boldsymbol{A}}_t^r, r)}\right]. \tag{2.43}$$

If one defines starting values in terms of the randomly sampled initial-boundary data

$$\tilde{\mathbf{p}}(\boldsymbol{x}, 0 \vee \tilde{\sigma}_t(\boldsymbol{x})) := \mathbf{p}_{dat} \left( \tilde{\boldsymbol{A}}_t^{0\prime}(\boldsymbol{x}), 0 \vee \tilde{\sigma}_t(\boldsymbol{x}) \right), \tag{2.44}$$

and defines at later times

$$\tilde{\mathbf{p}}(\boldsymbol{x},\tau) := \text{Texp}\left[-\int_{0\vee\tilde{\sigma}_{t}(\boldsymbol{x})}^{\tau} dr \ (\boldsymbol{\nabla}_{x}\boldsymbol{u})|_{(\widetilde{\boldsymbol{A}}_{t}^{r},r)}\right] \tilde{\mathbf{p}}(\boldsymbol{x},0\vee\tilde{\sigma}_{t}(\boldsymbol{x})), \qquad t > \tau > 0\vee\tilde{\sigma}_{t}(\boldsymbol{x}),$$
(2.45)

then the stochastic representation in Lemma 5.1 can be expressed simply as

$$\mathbf{p}(\boldsymbol{x},t) = \mathbb{E}\left[\tilde{\mathbf{p}}(\boldsymbol{x},t)\right]. \tag{2.46}$$

However, by direct differentiation of the matrix exponential in (2.45) one can see that

$$\frac{d}{d\tau}\tilde{\mathbf{p}}(\boldsymbol{x},\tau) = -\left(\boldsymbol{\nabla}_{x}\boldsymbol{u}\right)|_{(\widetilde{\boldsymbol{A}}_{t}^{T},\tau)}\tilde{\mathbf{p}}(\boldsymbol{x},\tau), \qquad t > \tau > 0 \lor \tilde{\sigma}_{t}(\boldsymbol{x}). \tag{2.47}$$

This appears exactly the same as the Lie-transport equation of a 1-form except that the material derivative  $D_{\tau}$  has been replaced with the time-derivative  $\partial/\partial \tau$  along the random trajectory  $\tilde{\boldsymbol{A}}_{t}^{\tau}(\boldsymbol{x})$  starting at  $\tau=0 \vee \tilde{\sigma}_{t}(\boldsymbol{x})$  and ending at  $\tau=t$ . We thus see that the randomly sampled initial-boundary data  $\tilde{\mathbf{p}}(0\vee\tilde{\sigma}_{t}(\boldsymbol{x}))$  is quasi-Lie-transported as a 1-form along stochastic trajectories forward in time to point  $(\boldsymbol{x},t)$  and the resulting contributions  $\tilde{\mathbf{p}}(\boldsymbol{x},t)$  are averaged over the ensemble to yield  $\mathbf{p}(\boldsymbol{x},t)$ . The process is illustrated in Fig. 1. In this stochastic Lagrangian representation, the quasi-Lie-transport along stochastic trajectories represents the nonlinear dynamics of vortex-momentum under the Kuz'min-Oseledets equation and cancellations in the ensemble average represent the destruction of vortex-momentum by viscosity. The analogous interpretation holds for the vorticity

representation in Proposition 6.1. Using the similar matrix exponential

$$(\boldsymbol{\nabla}_{x}\widetilde{\boldsymbol{A}}_{t}^{s})^{\top - 1} = \text{Texp}\left[\int_{s}^{t} dr \ (\boldsymbol{\nabla}_{x}\boldsymbol{u})^{\top}|_{(\widetilde{\boldsymbol{A}}_{t}^{r},r)}\right],$$
 (2.48)

one can show that randomly sampled initial-boundary data

$$\tilde{\boldsymbol{\omega}}(\boldsymbol{x}, 0 \vee \tilde{\sigma}_t(\boldsymbol{x})) = \boldsymbol{\omega}_{dat} \left( \tilde{\boldsymbol{A}}_t^{0\prime}(\boldsymbol{x}), 0 \vee \tilde{\sigma}_t(\boldsymbol{x}) \right)$$
(2.49)

are quasi-Lie-transported along stochastic trajectories  $\tilde{\boldsymbol{A}}_t^{\tau}(\boldsymbol{x})$  from  $\tau = 0 \vee \tilde{\sigma}_t(\boldsymbol{x})$  to  $\tau = t$  according to the equation

$$\frac{d}{d\tau}\tilde{\boldsymbol{\omega}}(\boldsymbol{x},\tau) = (\tilde{\boldsymbol{\omega}}(\boldsymbol{x},\tau) \cdot \boldsymbol{\nabla}_{x})\boldsymbol{u}|_{(\tilde{\boldsymbol{A}}_{t}^{\tau},\tau)}, \qquad t > \tau > 0 \vee \tilde{\sigma}_{t}(\boldsymbol{x}), \tag{2.50}$$

which closely resembles the usual inviscid evolution equation for vorticity. The final contributions at  $\tau = t$  are then averaged over the ensemble to give the resultant vorticity

$$\omega(x,t) = \mathbb{E}\left[\tilde{\omega}(x,t)\right],\tag{2.51}$$

and cancellations in this average over random contributions represent the viscous destruction of vorticity in a Lagrangian framework.

Although the physical interpretation is made more transparent by integrating forward in time, the method of proof integrating backward in time yields a more powerful result. It is obviously an arbitrary decision to make 0 the "initial time" and one can instead solve the viscous Kuz'min-Oseledets and Helmholtz equations starting at any time s < t with initial data  $\mathbf{p}(\cdot, s)$ . In that case, the same arguments as for s = 0 yield

$$\mathbf{p}(\boldsymbol{x}, t) = \mathbb{E}\left[\tilde{\mathbf{p}}_{\circ}(\boldsymbol{x}, t)\right], \quad s < t \tag{2.52}$$

with

$$\tilde{\mathbf{p}}_{s}(\boldsymbol{x},t) := \nabla_{x} \tilde{\boldsymbol{A}}_{t}^{s\prime}(\boldsymbol{x}) \cdot \mathbf{p} \left( \tilde{\boldsymbol{A}}_{t}^{s\prime}(\boldsymbol{x}), s \vee \tilde{\sigma}_{t}(\boldsymbol{x}) \right), \tag{2.53}$$

and likewise

$$\omega(\mathbf{x}, t) = \mathbb{E}\left[\tilde{\omega}_s(\mathbf{x}, t)\right], \quad s < t$$
 (2.54)

with

$$\widetilde{\boldsymbol{\omega}}_{s}(\boldsymbol{x},t) := (\boldsymbol{\nabla}_{x}\widetilde{\boldsymbol{A}}_{t}^{s\prime}(\boldsymbol{x}))^{\top - 1} \cdot \boldsymbol{\omega} \left( \widetilde{\boldsymbol{A}}_{t}^{s\prime}(\boldsymbol{x}), s \vee \widetilde{\sigma}_{t}(\boldsymbol{x}) \right). \tag{2.55}$$

The quantities  $\tilde{\mathbf{p}}_{c}(x,t)$  and  $\tilde{\omega}_{s}(x,t)$  defined above are the backward martingale random processes in s that were used in the proofs of Lemma 5.1 and Proposition 6.1, which are thus statistically conserved for every choice of  $x \in \Omega$ . If s = 0, then  $\tilde{\mathbf{p}}_0(x,t)$ ,  $\tilde{\omega}_0(x,t)$ are the same quantities  $\tilde{\mathbf{p}}(\mathbf{x},t)$ ,  $\tilde{\boldsymbol{\omega}}(\mathbf{x},t)$  that were introduced in discussing the physical interpretation using forward integration. The proofs in Constantin & Iyer (2011) thus provide an infinite set of stochastic Lagrangian conservation laws for incompressible Navier-Stokes solutions. We shall refer to  $\tilde{\omega}_s(x,t)$  for  $x \in \Omega$  and s < t, in particular, as the stochastic Cauchy invariants, since they generalize the Cauchy vorticity invariants of incompressible Euler solutions. See Frisch & Villone (2014) for historical perspective. One fundamental difference is that the Cauchy invariants for Euler are conserved both forward and backward in time, but the stochastic Cauchy invariants for Navier-Stokes are conserved only backward in time. This difference arises because the Navier-Stokes equation, unlike Euler, is time-irreversible and the stochastic Cauchy invariants express the fixed arrow of time. For this same reason, we have written the stochastic invariants as functions of the particle position "labels" x at the final time t rather than, as usual for ideal fluids, in terms of the particle positions a at early times s < t. As we shall see in the discussion of numerical methods in the next section, realizations of  $\tilde{\mathbf{p}}_s(\boldsymbol{x},t)$ ,  $\tilde{\boldsymbol{\omega}}_s(\boldsymbol{x},t)$  can be calculated for all s < t by a simple integration scheme backward in time using ensembles of stochastic Lagrangian particles. The requirement that their averages values remain independent of s is a stringent test on the accuracy of the numerics.

### 2.3. Relation with the Lighthill-Morton Theory

The Constantin & Iyer (2011) representation (2.54), (2.55) for any flow entirely bounded by walls allows one to reconstruct the interior vorticity  $\omega(\mathbf{x},t)$  at any point  $\mathbf{x} \in \Omega$  and time t in terms of the vorticity at the boundary, by taking the time interval t-s so large that  $\tilde{\sigma}_t(\mathbf{x}) > s$  with overwhelming probability. This formula thus makes very concrete the truism that all vorticity in the flow originates, ultimately, at a solid wall. The Constantin & Iyer (2011) theory does not address the generation of the wall-vorticity, but instead takes the boundary values  $\omega_W(\mathbf{x},t)$  for  $\mathbf{x} \in \partial \Omega$  as a given. It therefore plays a rather complementary role to the theory of Lighthill (1963) and Morton (1984), which was advanced to explain the inviscid generation of vorticity at the wall. The Constantin & Iyer (2011) formulas instead describe, in a Lagrangian framework, the subsequent transport of vorticity away from the walls by nonlinear advection, stretching and viscous diffusion. In order to discuss more clearly the relations of the two approaches, we must first review briefly the Lighthill-Morton theory, especially since some minor controversies still exist regarding its general formulation.

The concept of "vorticity source" or "vorticity flux density" was first introduced in the pioneering work of Lighthill (1963), who identified vorticity generation in an infinitesimal layer at a solid, stationary wall as an essentially inviscid process driven by tangential pressure gradients. Lighthill's theory was extended by Morton (1984) to accelerating walls, with the conclusion that the source of tangential vorticity at the wall is given by

$$\boldsymbol{\sigma} = \hat{\boldsymbol{n}} \times (\boldsymbol{\nabla}_x \boldsymbol{p} + D_t \boldsymbol{u})|_{\partial\Omega} \tag{2.56}$$

at least for a flow domain with a two-dimensional flat boundary and constant outward unit normal vector, say,  $\hat{\boldsymbol{n}} = -\hat{\mathbf{y}}$ . This quantity has dimensions of (vorticity)×(velocity). Concretely, by the Kelvin theorem,  $\boldsymbol{\sigma} \cdot \hat{\boldsymbol{n}} \times d\mathbf{l}$  represents the rate of generation of circulation along a small line-element  $d\mathbf{l} = \hat{\mathbf{t}} ds$ , with  $\hat{\mathbf{t}}$  any unit vector tangent to the wall, and thus  $\boldsymbol{\sigma} \cdot \hat{\boldsymbol{n}} \times \hat{\mathbf{t}}$  represents the wall-normal flux of vorticity generated in the direction  $\hat{\boldsymbol{n}} \times \hat{\mathbf{t}}$  (Morton 1984; Eyink 2008). Applying the momentum-balance (Navier-Stokes) equations at the wall, for the simplified two-dimensional geometry, Lighthill (1963) and Morton (1984) obtained alternative expressions for tangential vorticity source:

$$\sigma_x = -\nu \frac{\partial \omega_x}{\partial y} \bigg|_{\partial \Omega}, \quad \sigma_z = -\nu \frac{\partial \omega_z}{\partial y} \bigg|_{\partial \Omega}.$$
 (2.57)

These formulas express the instantaneous balance between rate of generation of vorticity at the wall and the rate of viscous diffusion of vorticity away from the wall. Using the facts that  $\partial \omega_y/\partial x|_{\partial\Omega}=0$  and  $\partial \omega_y/\partial z|_{\partial\Omega}=0$ , the latter expressions can be rewritten as

$$\boldsymbol{\sigma} = -\nu \hat{\boldsymbol{n}} \times (\boldsymbol{\nabla}_x \times \boldsymbol{\omega})|_{\partial\Omega} = \boldsymbol{\Sigma} \hat{\boldsymbol{n}}|_{\partial\Omega}, \qquad (2.58)$$

where  $\Sigma$  is the vorticity flux for Navier-Stokes defined in (1.2) as an anti-symmetric matrix. Since  $-\Sigma^{\top}\hat{n}$  represents generally the flux of vector vorticity in the space direction  $-\hat{n}$  (inward unit normal), the formula (2.58) has a natural physical interpretation and plausibly generalizes the Lighthill-Morton theory to flow domains with three-dimensional, curvilinear boundaries. This generalization was first proposed by Lyman (1990).

There is a subtlety, however, because the concept of "vorticity flux vector" is only

defined up to a divergence-free contribution, and the most standard choice of viscous flux is not the anti-symmetric tensor in (1.2) but is instead  $\Sigma'_{visc} = -\nu \nabla_x \omega$ . This yields

$$\boldsymbol{\sigma}' = -\boldsymbol{\Sigma}'^{\top} \hat{\boldsymbol{n}} \big|_{\partial\Omega} = \nu(\hat{\boldsymbol{n}} \cdot \boldsymbol{\nabla}_x) \boldsymbol{\omega} \big|_{\partial\Omega}, \tag{2.59}$$

which was suggested already by Panton (1984), sections 13.7, 13.11, and still often espoused (Wu & Wu 1993, 1996, 1998). There are obvious distinctions between the two proposals. In particular,  $\Sigma$  is anti-symmetric, so that  $\sigma \cdot \hat{n} = 0$  and thus Lyman's generalization predicts no generation of vorticity normal to the boundary. However, even for a flat, two-dimensional wall, typically  $\sigma' \cdot \hat{n} \neq 0$ . The latter result seems implausible, since wall-normal vorticity is associated to flux through loops lying entirely within the wall and pressure-gradients can drive no net circulation round such loops. However, we believe that a stronger argument in favor of  $\sigma$  rather than  $\sigma'$ , is that it is  $\Sigma$  which appears in the momentum balance (1.1) and not  $\Sigma'$ . Thus, it is only (2.58) which corresponds to the Lighthill-Morton inviscid expression (2.56) for a general three-dimensional boundary, and the Kelvin-theorem argument of Morton (1984) and Eyink (2008) then gives a spatially local meaning to  $\sigma$ . For this reason, we shall here adopt (2.56) and (2.58) as the generally correct formulation. Fortunately there is no difference in the predictions of the competing proposals of Lyman (1990) and Panton (1984) for the example which is studied numerically in this work, namely, the flux of tangential vorticity away from a flat, two-dimensional channel wall, so we may disregard this issue hereafter.

The Lighthill-Morton theory is directly related to the statistical result (1.4) derived by Taylor (1932) and Huggins (1994) for statistically stationary turbulence in domains with non-accelerating walls:

$$\overline{\Sigma}_{ij} = \epsilon_{ijk} \partial_k \overline{\left(p + \frac{1}{2} |\boldsymbol{u}|^2\right)}$$
 (2.60)

which locally relates vorticity flux and generalized pressure-gradients at interior points. The time-averaged tangential vorticity source relation of Lighthill-Morton:

$$\overline{\sigma}_i = \overline{\Sigma}_{ij} \hat{n}_j \Big|_{\partial\Omega} = (\hat{\boldsymbol{n}} \times \boldsymbol{\nabla}_x \overline{p})_i \Big|_{\partial\Omega}$$
 (2.61)

is just the Taylor-Huggins relation (2.60) approaching a boundary point and considering wall-normal flux of vorticity driven by mean tangential pressure-gradients. Here we note that there may be an average transport of tangential vorticity also parallel to the wall, driven by mean wall-normal gradients of generalized pressure:

$$\frac{\partial}{\partial n} \overline{p + (1/2)|\boldsymbol{u}|^2} \Big|_{\partial\Omega} = \frac{1}{2} \epsilon_{ijk} \hat{n}_i \overline{\Sigma}_{jk} \Big|_{\partial\Omega} = -\nu (\hat{\boldsymbol{n}} \times \boldsymbol{\nabla}_x) \cdot \overline{\boldsymbol{\omega}} \Big|_{\partial\Omega}. \tag{2.62}$$

The above relation is just the time-average of the standard Neumann boundary condition on the pressure (noting that  $(\partial/\partial n)|u|^2 = 0$  at the wall). The Taylor-Huggins result (2.60) continues both of the time-averaged relations (2.61) and (2.62) into the interior of the flow, where the vorticity current tensor in (1.2) for an incompressible Navier-Stokes fluid takes the form:

$$\Sigma_{ij} = u_i \omega_j - u_j \omega_i + \nu \left( \frac{\partial \omega_i}{\partial x_j} - \frac{\partial \omega_j}{\partial x_i} \right), \tag{2.63}$$

with contributions not only from viscous diffusion but also from nonlinear advection and stretching by the fluid flow velocity.

The Constantin-Iyer formalism provides a Lagrangian description of the space-transport of vorticity, with contributions from the same physical processes that are represented by the Eulerian vorticity current (2.63). The stochastic Cauchy invariant (2.55) can be di-

rectly related to the vorticity current by integration over any open subdomain  $O \subset \Omega$  with smooth boundary  $\partial O$  and by statistical expectation, yielding

$$\mathbb{E}\left[\int_{O} d^{3}x \left(\tilde{\boldsymbol{\omega}}_{s}(\boldsymbol{x},t) - \boldsymbol{\omega}(\boldsymbol{x},s)\right)\right] = \int_{s}^{t} dr \int_{\partial O} \boldsymbol{\Sigma}(\boldsymbol{x},r) \cdot d\mathbf{A}, \quad s < t, \tag{2.64}$$

where dA is the outward-pointing vector area element on  $\partial O$ . Of course, here  $\Sigma$  and  $\Sigma'$  yield the same total surface integral, as does any other vorticity current that differs from these two by a divergence-free vector. Detailed understanding of the physical processes contributing in the Constantin-Iyer representation can be obtained by decomposing

$$\left(\tilde{\boldsymbol{\omega}}_{s}(\boldsymbol{x},t) - \boldsymbol{\omega}(\boldsymbol{x},s)\right) = \left(\boldsymbol{\omega}(\tilde{\boldsymbol{A}}_{t}^{s}(\boldsymbol{x}),s) - \boldsymbol{\omega}(\boldsymbol{x},s)\right) + \left(\tilde{\boldsymbol{\omega}}_{s}(\boldsymbol{x},t) - \boldsymbol{\omega}(\tilde{\boldsymbol{A}}_{t}^{s}(\boldsymbol{x}),s)\right). \quad (2.65)$$

The first term on the right of (2.65) represents spatial transport of vorticity by fluid advection and viscous diffusion, while the second term represents space transport by vortex-stretching. To see this, note that the space-integral of the first term gives

$$\int_{O} d^{3}x \left(\boldsymbol{\omega}(\widetilde{\boldsymbol{A}}_{t}^{s}(\boldsymbol{x}), s) - \boldsymbol{\omega}(\boldsymbol{x}, s)\right) = \int_{\widetilde{\boldsymbol{A}}_{t}^{s}(O)\backslash O} d^{3}x \ \boldsymbol{\omega}(\boldsymbol{x}, s) - \int_{O\backslash \widetilde{\boldsymbol{A}}_{t}^{s}(O)} d^{3}x \ \boldsymbol{\omega}(\boldsymbol{x}, s) \ (2.66)$$

for  $t>s>\tilde{\sigma}_t(O):=\sup_{\boldsymbol{x}\in O}\tilde{\sigma}_t(\boldsymbol{x})$ , because the stochastic flow preserves the volume elements in O before any particle hits the flow boundary. The expression on the right side of (2.66) transparently represents change of the space-integral by transport due to advection and viscous diffusion. Indeed, the integration set  $\widetilde{\boldsymbol{A}}_t^s(O)\backslash O$  consists of points outside O at time s that enter it by time t and their contribution has a positive sign, whereas the set  $O\backslash \widetilde{\boldsymbol{A}}_t^s(O)$  consists of points inside O at time s that leave it by time t and their contribution has a negative sign. Note furthermore from Constantin & Iyer (2011), Proposition 5.2 that

$$\lim_{s \to t-} \frac{1}{t-s} \mathbb{E} \left[ \boldsymbol{\omega} (\widetilde{\boldsymbol{A}}_{t}^{s}(\boldsymbol{x}), s) - \boldsymbol{\omega}(\boldsymbol{x}, s) \right] = -(\boldsymbol{u}(\boldsymbol{x}, t) \cdot \nabla) \boldsymbol{\omega}(\boldsymbol{x}, t) + \nu \triangle \boldsymbol{\omega}(\boldsymbol{x}, t)$$
$$= -\nabla \cdot \left[ \boldsymbol{u} \boldsymbol{\omega} + \boldsymbol{\Sigma}_{visc} \right]$$
(2.67)

with  $\Sigma_{visc} = -\nu \left[ (\nabla \omega) - (\nabla \omega)^{\top} \right]$ . The first term in (2.65) thus recovers the instantaneous contributions to  $\Sigma$  from advection and viscous diffusion in the limit  $s \to t$ . On the other hand, the second term in (2.65) can be rewritten using the definition (2.55) of the stochastic Cauchy invariant, as:

$$\left(\widetilde{\boldsymbol{\omega}}_{s}(\boldsymbol{x},t) - \boldsymbol{\omega}(\widetilde{\boldsymbol{A}}_{t}^{s}(\boldsymbol{x}),s)\right) = \left[\left(\boldsymbol{\nabla}_{x}\widetilde{\boldsymbol{A}}_{t}^{s}(\boldsymbol{x})\right)^{\top - 1} - \mathbf{I}\right] \cdot \boldsymbol{\omega}\left(\widetilde{\boldsymbol{A}}_{t}^{s}(\boldsymbol{x}),s\right), \tag{2.68}$$

for  $t > s > \tilde{\sigma}_t(\boldsymbol{x})$ . The vector  $\boldsymbol{\omega}\left(\widetilde{\boldsymbol{A}}_t^s(\boldsymbol{x}), s\right)$  represents the initial vorticity sampled at time s, while the matrix  $(\boldsymbol{\nabla}_x \widetilde{\boldsymbol{A}}_t^s(\boldsymbol{x}))^{\top - 1} - \mathbf{I}$  represents the accumulated change from stretching and rotation between times s and t, as illustrated by the middle panel of Figure 1. Note that it follows either from the equation of motion (2.37) for  $\boldsymbol{\nabla}_x \widetilde{\boldsymbol{A}}_t^s(\boldsymbol{x})$  or from the closed expression (2.48) in terms of a time-ordered exponential, that

$$\lim_{s \to t-} \frac{1}{t-s} \left( (\boldsymbol{\nabla}_x \widetilde{\boldsymbol{A}}_t^s(\boldsymbol{x}))^{\top - 1} - \mathbf{I} \right) \cdot \boldsymbol{\omega} \left( \widetilde{\boldsymbol{A}}_t^s(\boldsymbol{x}), s \right) = (\boldsymbol{\omega}(\boldsymbol{x}, t) \cdot \boldsymbol{\nabla}) \boldsymbol{u}(\boldsymbol{x}, t),$$

$$= -\boldsymbol{\nabla} \cdot \left[ -\boldsymbol{\omega} \boldsymbol{u} \right]. \tag{2.69}$$

Thus, the second term in (2.65) recovers the instantaneous vortex-stretching contribution to  $\Sigma$  in the limit  $s \to t-$ . Combining (2.67) and (2.69) gives

$$\lim_{s \to t_{-}} \frac{1}{t - s} \mathbb{E} \left[ \tilde{\omega}_{s}(\boldsymbol{x}, t) - \boldsymbol{\omega}(\boldsymbol{x}, s) \right] = -\boldsymbol{\nabla} \cdot \boldsymbol{\Sigma}, \tag{2.70}$$

which is a spatially local version of (2.64) for infinitesimal times.

While the analysis of Constantin & Iyer (2008, 2011) takes the vorticity at the wall as Dirichlet boundary data for the Helmholtz equation, a more direct connection with the Lighthill-Morton theory can be established by taking instead the vorticity source density (2.58)-(2.59) as Neumann data. This generalization follows by utilizing stochastic Lagrangian trajectories reflected at the wall and the concept of "boundary local-time density" as in Drivas & Eyink (2017), but the mathematical derivation and numerical implementation must be deferred to a following work (Eyink et al. 2020b). In the application to channel-flow turbulence in paper II, the preceding discussion implies a constant average transport of spanwise vorticity by the stochastic Lagrangian flow in the wall-normal direction, with the vorticity flux driven by pressure-drop downstream in the channel. One of the main long-term goals of our program of study is a detailed Lagrangian description of the dynamical processes contributing to this systematic vorticity transport.

### 3. Numerical Methods and Their Evaluation

The mathematical theory discussed above can be implemented numerically in a straightforward fashion. We outline below a simple algorithm to calculate realizations of the stochastic Cauchy invariants and to evaluate their statistical averages, given the velocity and velocity-gradient fields associated to any solution of the incompressible Navier-Stokes equation. This algorithm is then implemented with an online database of a turbulent channel-flow solution (Graham et al. 2016), validating our computational method by verifying the conservation in the mean of the Cauchy vorticity invariant. In the following paper II we shall then exploit the stochastic Cauchy invariant to study numerically the Lagrangian vorticity dynamics for a couple of selected events in the buffer-layer of the channel-flow, allowing us to explicate in detail the origin of the vorticity at the wall.

Let us note in passing that the stochastic Lagrangian formulation can also be employed in principle as a numerical method for a priori calculation of Navier-Stokes solutions as Eulerian velocity fields. It is possible to obtain such solutions through a nonlinear fixed point-iteration, by making an initial guess of the space-time velocity field, solving equation (2.33) for the stochastic back-to-label maps, and then ensemble-averaging and Leray-projecting in (2.35) to obtain the next iteration of the velocity field (see Iyer (2006), section 3.2). However, this iteration scheme would be far less efficient than standard numerical discretization methods for computing Navier-Stokes solutions and we believe it has no promise for that purpose. The forefront numerical application of the stochastic Lagrangian formulation is instead for post-analysis of space-time data from prior Navier-Stokes computations and laboratory experiments.

## 3.1. Numerical Monte Carlo Lagrangian Scheme

The numerical method we will elaborate is based on a straightforward time-discretization of the stochastic differential equations (2.33) for the "back-to-labels" maps, or the histories of stochastic Lagrangian particles backward in time. We use the Euler-Maruyama method to calculate stochastic particle positions  $\tilde{\boldsymbol{A}}_t^s = (\tilde{a}_t^s, \tilde{b}_t^s, \tilde{c}_t^s)$  over discrete times  $s = s_k := t - k(\Delta s), \ k = 0, 1, 2, \dots$  by backward integration:

$$\widetilde{\boldsymbol{A}}_{t}^{s_{k}}(\boldsymbol{x}) = \widetilde{\boldsymbol{A}}_{t}^{s_{k-1}}(\boldsymbol{x}) - \boldsymbol{u}(\widetilde{\boldsymbol{A}}_{t}^{s_{k-1}}(\boldsymbol{x}), s_{k-1}) \Delta s + \sqrt{2\nu\Delta s} \, \widetilde{\mathbf{N}}^{k}, \quad k = 1, 2, 3, ...; \quad \widetilde{\boldsymbol{A}}_{t}^{t}(\boldsymbol{x}) = \boldsymbol{x}. \tag{3.1}$$

See Kloeden & Platen (2013). Here  $\tilde{\mathbf{N}}^k$  is a three-dimensional normal random vector with mean zero and covariance matrix  $\mathbf{I}$ , independently sampled for each step k = 1, 2, 3, ... For additive noise, as in the equation (3.1), the Euler-Maruyama scheme is first-order

strongly convergent as  $\Delta s \to 0$ . We use the Mersenne Twister algorithm (Matsumoto & Nishimura 1998; Matsumoto 1997-present) to produce a pseudo-random sequence of uniform random numbers and we generate samples of normal random numbers pairwise using the transform method of Box & Muller (1958). To numerically approximate the Cauchy invariant as defined in (2.55), or

$$\widetilde{\boldsymbol{\omega}}_{s}(\boldsymbol{x},t) = (\boldsymbol{\nabla}_{x}\widetilde{\boldsymbol{A}}_{t}^{s\prime}(\boldsymbol{x}))^{-1} \boldsymbol{\nabla}_{\omega}(\widetilde{\boldsymbol{A}}_{t}^{s\prime}(\boldsymbol{x}), s \vee \widetilde{\sigma}_{t}(\boldsymbol{x}))$$
(3.2)

we must also discretize the evolution equation for the deformation gradient tensors  $\widetilde{\boldsymbol{D}}_{t}^{s}(\boldsymbol{x}) := (\boldsymbol{\nabla}_{x}\widetilde{\boldsymbol{A}}_{t}^{s})^{-1}$ , or the Jacobian derivative matrices of the flow map. The equation for  $\widetilde{\boldsymbol{D}}_{t}^{s}(\boldsymbol{x})$  was already derived in (2.41) and is reproduced here

$$d\widetilde{\boldsymbol{D}}_{t}^{s} = -\widetilde{\boldsymbol{D}}_{t}^{s} \cdot (\nabla_{x} \boldsymbol{u})^{\top} \Big|_{(\widetilde{\boldsymbol{A}}_{t}^{s}, s)} ds, \quad s < t; \qquad \widetilde{\boldsymbol{D}}_{t}^{t} = \mathbf{I}$$
(3.3)

with the corresponding Euler approximation

$$\widetilde{\boldsymbol{D}}_{t}^{s_{k}} = \widetilde{\boldsymbol{D}}_{t}^{s_{k-1}} \cdot \left[ \mathbf{I} + (\boldsymbol{\nabla}_{x} \boldsymbol{u})^{\top} \big|_{(\widetilde{\boldsymbol{A}}_{t}^{s_{k-1}}, s_{k-1})} \Delta s \right], \quad k = 1, 2, 3, ...; \qquad \widetilde{\boldsymbol{D}}_{t}^{t} = \mathbf{I}.$$
 (3.4)

To calculate averages, a statistically independent ensemble of N stochastic Lagrangian particles is evolved, with positions  $\widetilde{\boldsymbol{A}}_t^{s_k,(n)}(\boldsymbol{x})$  and deformation matrices  $\widetilde{\boldsymbol{D}}_t^{s_k,(n)}(\boldsymbol{x})$  for n=1,...,N. At every kth-step in time s, Navier-Stokes solution fields  $\boldsymbol{u}$  and  $\nabla_x \boldsymbol{u}$  must be evaluated at the current set of particle locations and used to evolve both them and the deformation matrices backward to the next time. At each time-step k, the algorithm checks whether the nth particle has left the domain:

$$|\tilde{b}_t^{s_k,(n)}(\boldsymbol{x})| > h. \tag{3.5}$$

If so, this *n*th particle is declared to have been "born" at that time and evolved no further backward. Interpolation is used to identify the wall-hitting time  $s = \tilde{\sigma}_*^{(n)} = s_{k-1} - \Delta \tilde{\sigma}_*^{(n)}$  at which the condition  $|\tilde{b}_t^{s,(n)}(\boldsymbol{x})| = h$  first occurred. Note that  $\tilde{\sigma}_*^{(n)}$  is a random quantity, even given both  $\tilde{A}_t^{s_{k-1},(n)}(\boldsymbol{x})$  and  $\tilde{A}_t^{s_k,(n)}(\boldsymbol{x})$ . As discussed in Appendix A, this hitting time can be estimated by a stochastic interpolation method that becomes exact in the limit of a vanishing wall-normal velocity, with no restriction whatsoever on the time-step  $\Delta s$ . The same interpolation scheme gives also the wall positions  $(a,c)=(\tilde{a}_*^{(n)},\tilde{c}_*^{(n)})$  at the first-hitting time. Furthermore, the deformation matrix is updated to the hitting time by the Euler formula with a fractional time-step:

$$\widetilde{\boldsymbol{D}}_{t}^{\widetilde{\sigma}_{*}^{(n)},(n)} = \widetilde{\boldsymbol{D}}_{t}^{s_{k-1},(n)} \cdot \left[ \mathbf{I} + (\boldsymbol{\nabla}_{x}\boldsymbol{u})^{\top} \Big|_{(\widetilde{\boldsymbol{A}}_{t}^{s_{k-1},(n)},s_{k-1})} \Delta \widetilde{\sigma}_{*}^{(n)} \right]$$
(3.6)

and used to evaluate the Cauchy invariant for the newly "born" particle by the formula

$$\tilde{\boldsymbol{\omega}}_{*}^{(n)} = \tilde{\boldsymbol{D}}_{t}^{\tilde{\sigma}_{*}^{(n)},(n)} \cdot \boldsymbol{\omega}(\tilde{a}_{*}^{(n)}, \tilde{b}_{*}^{(n)}, \tilde{c}_{*}^{(n)}, \tilde{\sigma}_{*}^{(n)}), \quad \tilde{b}_{*}^{(n)} = \pm h$$
(3.7)

requiring the velocity-gradient  $\nabla_x u$  of the Navier-Stokes solution at space-time point  $(\tilde{a}_*^{(n)}, \tilde{b}_*^{(n)}, \tilde{c}_*^{(n)}, \tilde{\sigma}_*^{(n)})$ . The random values for each newly "born" particle with label n,

$$\tilde{\sigma}_{*}^{(n)}, \ \tilde{a}_{*}^{(n)}, \ \tilde{c}_{*}^{(n)}, \ \tilde{\omega}_{*}^{(n)},$$
 (3.8)

are then output to a file. Subsequently, for all of the remaining particles n, the so-called "alive" ones which have not yet hit the wall, the deformation matrix is updated by the Euler formula (3.4) to the new time  $s_k = s_{k-1} - \Delta s$  and then that matrix is used to

calculate an updated Cauchy invariant at time  $s_k$  with

$$\widetilde{\boldsymbol{\omega}}_{s_k}^{(n)}(\boldsymbol{x},t) = \widetilde{\boldsymbol{D}}_t^{s_k,(n)} \cdot \boldsymbol{\omega}(\widetilde{\boldsymbol{A}}_t^{s_k}(\boldsymbol{x}), s_k), \tag{3.9}$$

requiring the Navier-Stokes velocity-gradient  $\nabla_x u$  at time  $s_k$  to obtain  $\omega(\widetilde{A}_t^{s_k}(x), s_k)$ .

This entire procedure is repeated in all subsequent time-steps. The set of stochastic particles labelled by  $n \in \mathbb{N} = \{1, 2, ..., N\}$  is partitioned into a subset  $\mathbb{W}_k$  representing "wall"/"pre-born" particles that have already hit the wall by time-step k and the complementary subset  $\mathbb{I}_k = \mathbb{N} \backslash \mathbb{W}_k$  representing "interior" /"alive" particles still in the flow interior at time-step k. At each step, the variables associated to "wall" particles with  $n \in \mathbb{W}_k$  are left unchanged and only the variables associated to "interior" particles with  $n \in \mathbb{I}_k$  are evolved from time  $s_k$  back to time  $s_{k+1}$ . Identifying the newly "born" particles, storing the values of their variables at their first-hitting time, and adding their indices n to  $\mathbb{W}_k$  then yields the new sets  $\mathbb{W}_{k+1} \supseteq \mathbb{W}_k$  and  $\mathbb{I}_{k+1} = \mathbb{N} \backslash \mathbb{W}_{k+1}$  for the next time-step. At every step, ensemble-means of random variables  $\tilde{F}$  are calculated by averaging over the entire set of particles  $\mathbb{N}$ , both wall and interior, as:

$$\mathbb{E}[\tilde{F}] \doteq \frac{1}{N} \sum_{n=1}^{N} \tilde{F}^{(n)} \tag{3.10}$$

The convergence rate of this scheme as  $N \to \infty$  is rather slow, with standard Monte Carlo errors by the central limit theorem of order  $\sim \sqrt{\mathrm{Var}[F]/N}$ , where  $\mathrm{Var}[F]$  is the variance of the averaged variable. To obtain numbers of samples N sufficiently large, we implemented the preceding algorithm in Fortran on a cluster computer at the Maryland Advanced Research Computing Center (MARCC). The Monte Carlo averaging scheme is perfectly parallelizable, with statistically independent subsets of samples assigned to distinct cluster nodes and no communication whatsoever required between nodes.

An annotated version of the Fortran code which implements the algorithm discussed above is available at the Github repository (Eyink *et al.* 2019). This code is written to be used with the JHU online channel-flow database, which is discussed next.

### 3.2. JHU Channel-Flow Database

The Johns Hopkins Turbulence Databases (JHTDB) channel-flow dataset (Graham et al. 2016) is exploited for the empirical study in this paper. This data was generated from a Navier-Stokes simulation in a channel using a pseudospectral method in the plane parallel to the walls and a seventh-order B-splines collocation method in the wall-normal direction (Lee et al. 2013). For numerical solution, the Navier-Stokes equations were formulated in wall-normal velocity-vorticity form (Kim et al. 1987). Pressure was computed by solving the pressure Poisson equation only when writing to disk, which was every five time steps for 4000 snapshots, enough for about one domain flow-through time. The simulation domain  $[0,8\pi] \times [-h,h] \times [0,3\pi]$  with channel half-height h=1 was discretized using a spatial grid of  $2048 \times 512 \times 1536$  points in the streamwise (x), wall-normal (y), and spanwise (z) directions, respectively. Time advancement was made with a third-order low-storage Runge-Kutta method and dealiasing was performed with 2/3 truncation (Orszag 1971). A constant pressure head was applied to drive the flow at  $Re_{\tau} = 1000$  $(Re_{bulk} = \frac{2hU_{bulk}}{\nu} = 40\,000)$  with bulk velocity near unity. As is common, we shall indicate with a superscript "+" non-dimensionalized quantities in viscous wall units, with velocities scaled by friction velocity  $u_*$  and lengths by viscous length  $\delta_{\nu} = \nu/u_* = 10^{-3}$ . Also as usual, we define  $y^+ = (h \mp y)/\delta_{\nu}$  near  $y = \pm h$ . In these units, the first y-grid point in the simulation is located at distance  $\Delta y_1^+ = 1.65199 \times 10^{-2}$  from the wall, while in the

Table 1: Simulation Parameters for Turbulent Channel-Flow Dataset

$$N_x$$
  $N_y$   $N_z$   $Re_{\tau}$   $dp/dx$   $\nu$   $u_*$   $U_{bulk}$   $\Delta x^+$   $\Delta z^+$   $\Delta t$   
2048 512 1536 1000  $-2.5 \times 10^{-3}$   $5 \times 10^{-5}$   $5 \times 10^{-2}$  1.00 12.3 6.1  $1.3 \times 10^{-3}$ 

center of the channel  $\Delta y_c^+ = 6.15507$ . Other numerical parameters of the channel-flow dataset are summarized in Table 1.

The JHTDB Web services supports subroutine-like calls for data that can be made from MATLAB, Fortran, and C/C++ programs, including get Velocity for stored velocity data and getVelocityGradient for finite-difference approximations to velocity-gradients; see Li et al. (2008); Graham et al. (2016). To return data off the numerical space-time grid, the JHTDB Web services provide methods for performing spatial and temporal interpolation within the database. Spatial interpolation is supported using multivariate polynomial interpolation in the barycentric Lagrange form, with stencils containing q=4,6,8 points in each coordinate direction for an order q interpolant, so-called Lag4, Lag6, Lag8 methods, respectively. Temporal interpolation is supported using cubic Hermite interpolating polynomials (PCHIPInt), with centered finite-difference evaluation of the end-point time derivatives, employing a total of four temporal points. Spatial differentiation at grid points is performed using differentiation matrices obtained from the barycentric method of Lagrange polynomial interpolation for q = 4, 6, 8 points, socalled FD4NoInt, FD6NoInt, FD8NoInt options (Berrut & Trefethen 2004; Graham et al. 2016). The FD4Lag4 option provides off-grid space-interpolated gradients with derivatives approximated by the FD4NoInt method at the grid sites and these data then spaceinterpolated to queried points using the Lag4 method. In the current study, qet Velocity is used with Lag6 and PCHIPInt options to obtain off-grid velocity data and getVelocityGradient is used with FD4Lag4 and PCHIPInt options to obtain velocity-gradients.

Because the JHTDB turbulent channel-flow dataset was obtained from a numerical simulation with relatively low near-wall resolutions in the streamwise and spanwise directions (see Table 1), the vorticity  $\omega(x,t)$  returned by the database in the vicinity of the wall may exhibit observable departures from an exact Navier-Stokes solution. The stochastic Cauchy invariant approximated by equations (3.7), (3.9) thus cannot be expected to be exactly conserved in time using such numerical data, even if the stochastic Lagrangian integration scheme has  $\Delta s$  sufficiently small and N sufficiently large to be very well converged, since discretization errors depending upon  $\Delta x$ ,  $\Delta y$ ,  $\Delta z$ ,  $\Delta t$  will remain. On the other hand, a coarse-grained vorticity field

$$\widehat{\boldsymbol{\omega}}(\boldsymbol{x},t) = \int d^3x \ G_{\ell_x}(x-x')G_{\ell_y}(y-y')G_{\ell_z}(z-z') \ \boldsymbol{\omega}(\boldsymbol{x}',t)$$
(3.11)

when calculated from the database, with length-scales  $\ell_x$ ,  $\ell_y$ ,  $\ell_z$  each comprising several grid-lengths  $\Delta x$ ,  $\Delta y$ ,  $\Delta z$ , will plausibly agree with a Navier-Stokes solution coarse-grained over the same length-scales, with better correspondence than for pointwise fields. Of course, the coarse-grained stochastic Cauchy invariants for a Navier-Stokes solution

$$\hat{\tilde{\boldsymbol{\omega}}}_s(\boldsymbol{x},t) = \int d^3x \ G_{\ell_x}(x-x')G_{\ell_y}(y-y')G_{\ell_z}(z-z') \ \tilde{\boldsymbol{\omega}}_s(\boldsymbol{x}',t)$$
(3.12)

will satisfy a corresponding statistical conservation law

$$\widehat{\boldsymbol{\omega}}(\boldsymbol{x},t) = \mathbb{E}\left[\widehat{\widetilde{\boldsymbol{\omega}}}_s(\boldsymbol{x},t)\right] \tag{3.13}$$

Table 2: Coordinates of Analyzed Vorticity Vectors

	x	y	z	t	$\omega_x$	$\omega_y$	$\omega_z$
ejection	21.094707	0.994647	7.563944	25.9935	-2.24948978	-0.110395804	22.1811829
sweep	0.715000	0.995100	0.725900	25.9935	0.05745593	-0.1597188	47.2303467

as a direct consequence of the conservation of the fine-grained invariants. If the conjecture is correct that the coarse-grained numerical solutions will agree well with a coarse-grained exact Navier-Stokes solution, then we may expect to observe better conservation numerically for the coarse-grained invariants. To test this hypothesis in our study below, we shall use box/tophat filters with  $\ell_i = n_i(\Delta x_i)$  for integers  $n_i$ , i = x, y, z. In practice, this means that we locate the grid-point  $x_k$  that lies closest to a given point x and then average over the set of points x' in the box centered at  $x_k$  and extending  $n_i/2$  grid spacings to the left and to the right in each coordinate direction i = x, y, z. This space-average is easily included in our Monte Carlo scheme, by releasing stochastic Lagrangian particles at time t with positions x' chosen at random, uniformly distributed over such a box.

### 3.3. Validation of the Numerical Method

We shall now validate the computational algorithms described above by verifying the mean conservation law of the stochastic Cauchy invariant, Eq.(2.54). This is a stringent test of our numerical methods to evaluate the Cauchy invariant and its statistics and also of the fidelity of the JHTDB channel-flow dataset to a true Navier-Stokes solution.

## 3.3.1. Description of the Test Events and Variables

Before presenting numerical results, we must recall that the stochastic Cauchy invariant is a *vector* quantity, each of whose components  $\tilde{\omega}_{si}(\boldsymbol{x},t)$  for i=x,y,z is conserved on average, with mean value equal to  $\omega_i(\boldsymbol{x},t)$  independent of s< t. A coordinate-free decomposition of the stochastic Cauchy invariant can be obtained using the unit vector  $\hat{\boldsymbol{n}}_{\omega}(\boldsymbol{x},t):=\boldsymbol{\omega}(\boldsymbol{x},t)/|\boldsymbol{\omega}(\boldsymbol{x},t)|$  pointing in the direction of vorticity at final time t, which permits definition of parallel and perpendicular components of the Cauchy invariant

$$\widetilde{\omega}_{s\parallel}(\boldsymbol{x},t) := \widetilde{\boldsymbol{\omega}}_{s}(\boldsymbol{x},t) \cdot \hat{\boldsymbol{n}}_{\omega}(\boldsymbol{x},t), \quad \widetilde{\boldsymbol{\omega}}_{s\perp}(\boldsymbol{x},t) := \widetilde{\boldsymbol{\omega}}_{s}(\boldsymbol{x},t) - \widetilde{\omega}_{s\parallel}(\boldsymbol{x},t)\hat{\boldsymbol{n}}_{\omega}(\boldsymbol{x},t), \quad (3.14)$$

which satisfy the mean conservation laws

$$\mathbb{E}\left[\widetilde{\omega}_{s\parallel}(\boldsymbol{x},t)\right] = |\boldsymbol{\omega}(\boldsymbol{x},t)|, \quad \mathbb{E}\left[\widetilde{\boldsymbol{\omega}}_{s\perp}(\boldsymbol{x},t)\right] = \mathbf{0}, \quad s < t. \tag{3.15}$$

In our numerical study below we shall present results both for the Cartesian components of the stochastic Cauchy invariant and also for the intrinsic  $\parallel$ ,  $\perp$  components

We have selected for investigation from the channel-flow database two test vorticity vectors  $\omega(x,t)$ , whose detailed space-time coordinates are given in Table 2. The choice of these two cases is discussed in detail in paper II. Here it suffices to note that the spatial coordinates both correspond to points at the bottom of the buffer-layer, with  $y^+ \simeq 5$ , one at the location of an "ejection" where fluid is erupting away from the wall and the other at a "sweep" where fluid is splatting against the wall. We shall refer to these two events hereafter simply as the "ejection" and the "sweep", respectively.

### 3.3.2. Statistics of the Cauchy Invariant for the Ejection Event

We first consider the ejection case. In Fig. 2(a) we plot as functions of  $\delta s = s - t$  the numerically calculated expectation values of the *i*th component of the stochastic Cauchy

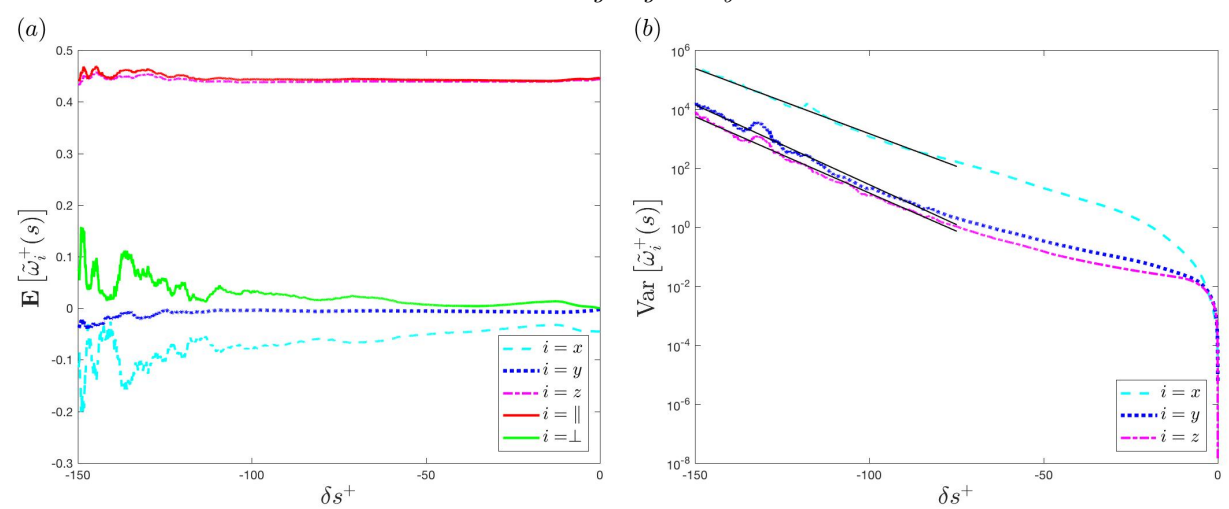


Figure 2: Expectation value (a) and variance (b) of the components  $\tilde{\omega}_{si}^+(\boldsymbol{x},t)$  of the stochastic Cauchy invariant for the selected point  $(\boldsymbol{x},t)$  in the ejection event, plotted as functions of  $\delta s^+$ , calculated numerically with  $\Delta s = 10^{-3}$  and  $N = 10^{7}$ . The thin black lines are linear fits in semilogarithmic coordinates for  $\delta s^+ < -75$ .

invariant for  $i=x,\,y,\,z,\,\parallel$ , and the vector norm  $|\mathbb{E}\left[\widetilde{\boldsymbol{\omega}}_{s\perp}(\boldsymbol{x},t)\right]|$  for  $i=\perp$ . These were obtained with the numerical Monte Carlo scheme in Section 3, using integration timestep  $\Delta s = 10^{-3}$  in Eqs.(3.1),(3.4) and number of particles  $N = 10^{7}$  to calculate sample averages as in Eq.(3.10). According to the mathematical theory for exact Navier-Stokes solutions presented in Section 2, the graphs for all components in Fig. 2(a) should be flat horizontal lines, with values equal to the corresponding components of the vorticity vector  $\omega(x,t)$  at the final time. While this is reasonably verified at  $\delta s^+ > -100$ , especially for components  $i = y, z, \parallel$ , there are clear deviations at longer times and for other components  $i = x, \bot$ . It should be emphasized that the "naive Cauchy invariants", which are exactly conserved for smooth Euler solutions, exhibit much larger deviations from conservation for the channel-flow Navier-Stokes solution than do the numerical results in Fig. 2(a) for the stochastic Cauchy invariants. As discussed in the SM, the "naive invariants" can be accurately evaluated by the same numerical methods as discussed in Section 3, by setting the random noise to zero and calculating a standard (deterministic) Lagrangian trajectory and the deformation matrix along it by a 4th-order Runge-Kutta scheme. The results in the SM show that conservation of the "naive invariants" is violated by several orders of magnitude for the same case as in Fig. 2(a). There is, of course, no reason that conservation of the standard Cauchy invariants should hold for any Navier-Stokes solution and the failure of conservation here confirms previous results that vorticity is not even approximately "frozen in" for a high Reynolds-number turbulent flow (Lüthi et al. 2005; Guala et al. 2005, 2006; Johnson & Meneveau 2016; Johnson et al. 2017). Nevertheless, despite the much better conservation of the stochastic Cauchy invariants that we observe, the deviations from exact conservation that arise in our various numerical approximations must be clearly understood.

A first possible source of error is the size of the time step. The value of  $\Delta s = 10^{-3}$  employed for stochastic integration was slightly smaller than the time-step  $\Delta t$  employed in the original channel-flow simulation archived in the database (see Table 1). Furthermore, as discussed in the SM, we checked that the numerical results with  $\Delta s = 10^{-3}$  are

essentially unchanged when using a twice smaller value  $\Delta s = 5 \times 10^{-4}$  over the reduced time range  $-100 < \delta s^+ < 0$ . The average difference over that interval between the values plotted in Fig. 2(a) and those generated with  $\Delta s = 5 \times 10^{-4}$  is less than 0.004 for all components. In particular, the average differences for the parallel and perpendicular components over that interval are, respectively, only 0.21% and 0.79% of the vorticity magnitude  $|\omega|$ . Thus, our results appear to be well-converged in the time-step.

A much larger source of numerical error in the results presented in Fig. 2(a) is the number of samples N employed to calculate averages over realizations of the Brownian motion. The error in approximating expectation values from N-sample averages as in Eq.(3.10) is estimated from the Central Limit Theorem on order of magnitude as

$$\delta \mathbb{E}\left[\widetilde{\omega}_{s\,i}(\boldsymbol{x},t)\right] \sim \sqrt{\frac{\operatorname{Var}\left[\widetilde{\omega}_{s\,i}(\boldsymbol{x},t)\right]}{N}}.$$
 (3.16)

We can numerically calculate the variances within the same Monte Carlo scheme by using the standard unbiased estimator

$$\operatorname{Var}[\tilde{F}] \doteq \frac{1}{N-1} \sum_{n=1}^{N} (\tilde{F}^{(n)} - \mathbb{E}[\tilde{F}])^2,$$
 (3.17)

and variances of the Cartesian coordinates of the stochastic Cauchy invariant estimated in this manner with  $\Delta s = 10^{-3}$ ,  $N = 10^7$  are plotted in Fig. 2(b) versus  $\delta s^+$ . After an initial transient period, these variances appear to grow exponentially rapidly backward in time, with  $\text{Var}[\widetilde{\omega}_{s\,i}(\boldsymbol{x},t)] \propto \exp(2\lambda_i(t-s))$  for  $s \ll t$ . The growth exponents obtained by linear fits of the numerical results over the range  $\delta s^+ < -75$  in semilogarithmic coordinates are

$$\lambda_x^+ = 0.0509, \quad \lambda_y^+ = 0.0624, \quad \lambda_z^+ = 0.0596.$$
 (3.18)

in wall units. Recall that, according to Eq. (2.50), the stochastic Cauchy invariant evolves in the same manner as does a material line element forward in time, except that the motion is along stochastic Lagrangian trajectories rather than deterministic ones. The exponential growth of variances that we find is thus consistent with the previous study of Johnson et al. (2017), who observed Lagrangian chaos in the same channel-flow database that we employ. The instantaneous Lyapunov exponents obtained by Johnson et al. (2017) are plotted in their Figure 4(b), with values  $2 \times 10^{-3} \sim 2 \times 10^{-2}$  in the range  $0 < y^{+} < 10$  where their non-dimensionalization by a local Kolmogorov time (increasing with y) corresponds essentially to our wall units. Our growth exponents for the variance are order of magnitude consistent with those Lyapunov exponents, but somewhat larger. The somewhat greater values could be due to the fact that we do not average over long times, as Johnson et al. (2017) did, and the local stretching rates in our extreme-stress event could be larger than average. Also, we do not conditionally sample on a given  $y^+$ value as Johnson et al. (2017) did, and the stochastic Lagrangian trajectories released at  $y^+ = 5.35$  can disperse into the buffer-layer where local stretching rates are highest (Johnson *et al.* 2017).

The errors in the mean values estimated from the Central Limit Theorem, using Eq. (3.16) and the variance calculated by Eq. (3.17), explain the largest deviations from exact conservation observed in Fig. 2(a). For  $\delta s^+ < -100$ , all of the observed deviations are consistent on order of magnitude with fluctuations due to finite N. Because of the slow Monte Carlo rate of convergence  $\propto 1/\sqrt{N}$  in Eq. (3.16), it would require  $N \simeq 10^{14}$  samples to achieve accuracy of even a few percent for  $\delta s^+ \simeq -150$ , which is beyond our computational means. On the other hand, we estimate from Eq. (3.16) that Monte Carlo errors are much less than 1% for  $\delta s^+ > -100$ . This is verified by the observed con-

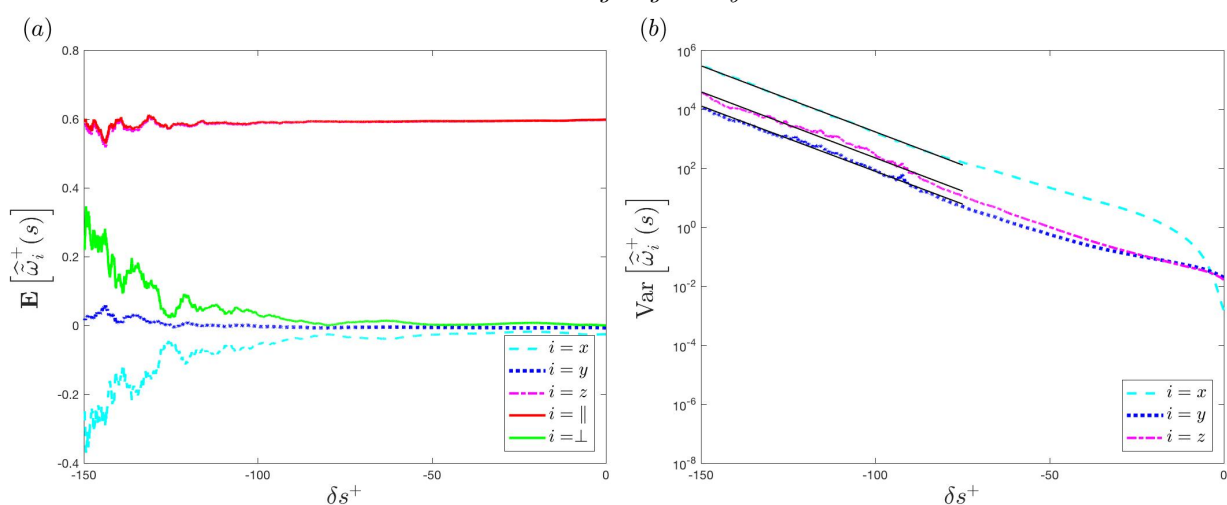


Figure 3: Expectation value (a) and variance (b) of the components  $\hat{\omega}_{si}^+(\boldsymbol{x},t)$  of the coarse-grained Cauchy invariant for the selected point  $(\boldsymbol{x},t)$  in the ejection event, plotted as functions of  $\delta s^+$ , calculated numerically with  $\Delta s = 10^{-3}$  and  $N = 10^{7}$ . The thin black lines are linear fits in semilogarithmic coordinates for  $\delta s^+ < -75$ .

vergence of the mean values with increasing N (not shown) and the smoothness of the plotted curves for  $\delta s^+ > -100$ . In that range, we see that the components  $i = y, z, \parallel$  of the stochastic Cauchy invariant are well conserved in the mean, but there are observable deviations from conservation for  $i = x, \perp$ . In fact, the mean deviation of the parallel and perpendicular components from conservation over the range  $-100 < \delta s^+ < 0$  are 0.57% and 2.97% of the magnitude  $|\omega|$ , respectively. The final-time vorticity direction vector is nearly  $\hat{\mathbf{n}}_{\omega} \simeq \hat{\mathbf{z}}$  for the case being examined, so that the error in conservation of the perpendicular component arises mainly from non-conservation of the x-component. These violations of exact conservation are not explained by any numerical artifacts of finite  $\Delta s$  and N in our Monte Carlo integration scheme.

The only remaining source of error in our computation is the deviation of the fields stored in the JHTDB channel-flow database from an exact Navier-Stokes solution. Although the numerical simulation stored in the database had excellent spatial resolution in the y-direction near the wall, the wall-parallel resolution was much poorer. As reviewed in Table 1,  $\Delta z^+ = 6.1$  and  $\Delta x^+ = 12.3$ . Furthermore, the velocity-gradients returned by the database function getVelocityGradient are finite-difference approximations and both velocities and velocity-gradients at points off the computational grid are supplied by Lagrangian interpolation. A reasonable estimate of the size of the errors involved in these approximations can be obtained from the deviation of the database velocity-gradient matrices from being traceless, as required by flow incompressibility. As we discuss in the SM, we have found that the divergence-free condition is satisfied to a few percent, with violation less than 0.5% for  $y^+ < 10$  but rising up to 3-4% for  $y^+ > 30$ . This inaccuracy in the returned velocity-gradients accords well with the magnitude of the deviations that we observe in mean conservation of the stochastic Cauchy invariant. An ensemble of stochastic Lagrangian particles released at  $y^+ = 5.35$  will sample not a resolved Navier-Stokes solution but instead a Lagrange interpolating polynomial, until the ensemble has dispersed over at least several grid-lengths in the wall-parallel directions. This is the presumed source of the slight non-conservation observed for  $i = x, \perp$ 

components at times  $\delta s^+ > -100$  in in Fig. 2(a). To test this explanation, we have numerically generated the coarse-grained stochastic Cauchy invariant defined in Eq. (3.12) for filter lengths  $\ell_i = n_i(\Delta x_i)$  in the coordinate directions, i = x, y, z, using the Monte Carlo scheme discussed in section 3.1. As discussed in paper II,  $(n_x, n_y, n_z) = (4, 0, 4)$  is a reasonable choice of filtering lengths which does not obscure the essential physics of the ejection event under consideration.

Plotted in Fig. 3 are the mean and variance of the coarse-grained stochastic Cauchy invariant for the selected point, filtered over  $(n_x, n_y, n_z) = (4, 0, 4)$  grid points. The fluctuations of the mean values for  $\delta s^+ < -100$  are increased compared with the unfiltered case shown in Fig. 2(a), because the empirical average over N samples is now doing double duty to represent both the expectation over the Brownian motion and the space-average over the filtering box. As can be seen from Fig. 3(b), the variances of the coarse-grained Cauchy invariant are somewhat increased relative to those plotted in Fig. 2(b), because the former include both stochastic and spatial fluctuations. On the other hand, as expected, the mean-conservation of the coarse-grained Cauchy invariant is observed in Fig. 3(a) to be improved for  $\delta s^+ > -100$  when compared with the finegrained means plotted in Fig. 2(a), especially for the  $i=x, \perp$  components. The average deviation from conservation of the parallel and perpendicular components is now found to be 0.79% and 1.22% of the magnitude  $|\widehat{\omega}|$ , respectively. We have found that increasing  $n_x$ ,  $n_z$  further (not shown) improves the mean conservation, while the spatial structures become more diffuse. Since mean conservation of the stochastic Cauchy invariant is a quite stringent test of validity of a Navier-Stokes solution, these results validate both our Monte Carlo numerical method to calculate the stochastic Cauchy invariant and also the adequacy of the JHTDB channel-flow database to investigate the turbulent buffer layer.

#### 3.3.3. Statistics of the Cauchy Invariant for the Sweep Event

We now consider, more briefly, the sweep event. We again investigate the mean conservation of the stochastic Cauchy invariant as a check on our numerical approximations. Fig. 4 plots the results for the mean and the variance of the components of the Cauchy invariant, calculated by our Monte Carlo integration scheme with time-step  $\Delta s = 10^{-3}$  and with number of samples  $N=10^7$ . As for the ejection event, we have performed a convergence analysis in  $\Delta s$  (see SM) and found that the results do not change significantly with a smaller time-step  $\Delta s = 5 \times 10^{-4}$ . Over the reduced interval  $-100 < \delta s^+ < 0$  the mean differences in results for the two time steps differ by less than 0.005 for all components and the mean differences for the parallel and perpendicular components are only 0.38% and 0.45% of the magnitude  $|\omega|$ , respectively. Due to the finite values of N, however, the results for  $\delta s^+ < -100$  exhibit very large errors, consistent with the variances plotted in Fig. 4(b). The results for  $-100 < \delta s^+ < 0$  on the other hand are well-converged in N, so that any residual errors there are due to lack of resolution in the archived channel-flow simulation. Mean conservation holds quite well for the y, z components of the stochastic Cauchy invariant in the time interval  $-100 < \delta s^+ < 0$  for this sweep event, but the x-component is less well conserved. Quantitatively, the mean deviations from conservation of the parallel and perpendicular components are 2.29\% and 5.01\% of the vorticity magnitude  $|\omega|$ , respectively. We have again found that spatial coarse-graining noticeably improves mean conservation, although a bit less well than it did in the ejection case. The mean deviations from conservation of the parallel and perpendicular components are now 1.43\% and 3.32\% of the vorticity magnitude  $|\widehat{\omega}|$ , respectively. We present plots of the coarse-grained stochastic Cauchy invariant for the sweep case in Fig. 5, where improved conservation can be observed especially for  $-50 < \delta s^+ < 0$ .

The growth exponents for the variances in the sweep case obtained by linear fits over

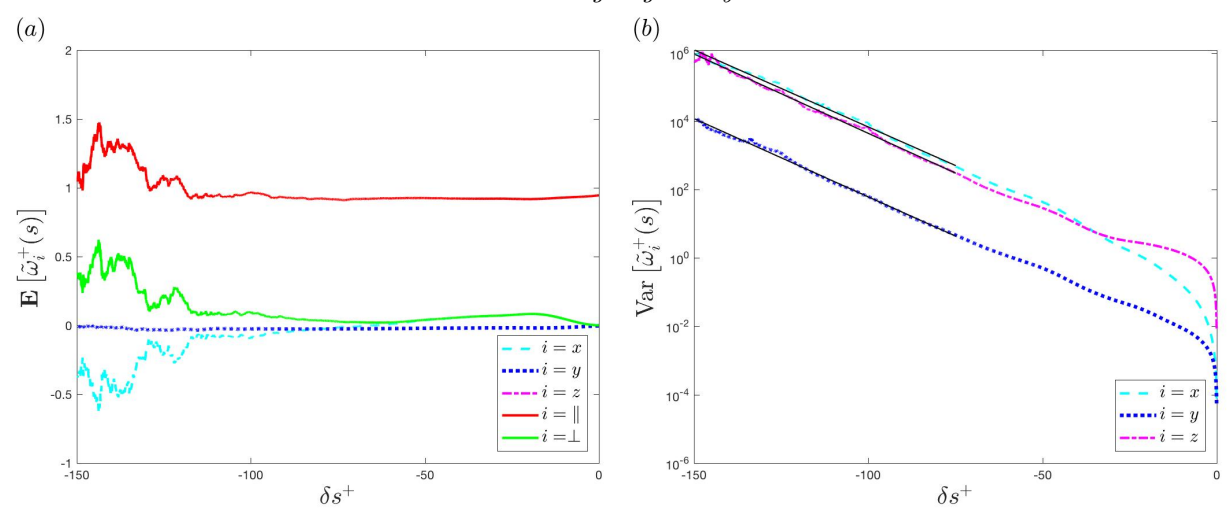


Figure 4: Expectation value (a) and variance (b) of the components  $\tilde{\omega}_{si}^+(\boldsymbol{x},t)$  of the stochastic Cauchy invariant for the selected point  $(\boldsymbol{x},t)$  in the sweep event, plotted as functions of  $\delta s^+$ , calculated numerically with  $\Delta s = 10^{-3}$  and  $N = 10^7$ . The thin black lines are linear fits in semilogarithmic coordinates for  $\delta s^+ < -75$ .

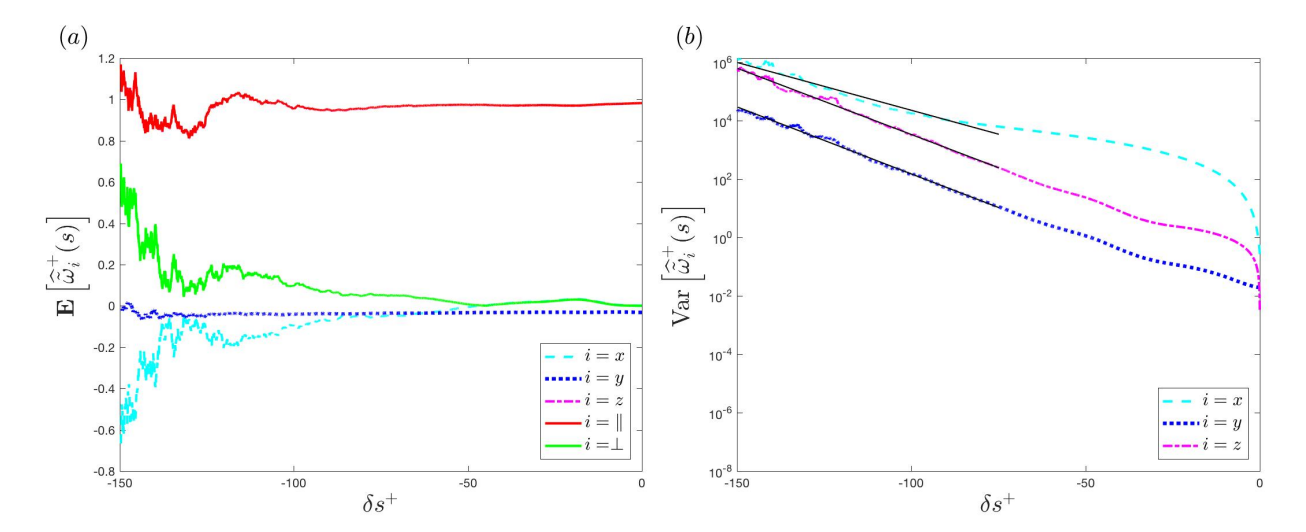


Figure 5: Expectation value (a) and variance (b) of the components  $\hat{\omega}_{si}^+(\boldsymbol{x},t)$  of the coarse-grained Cauchy invariant for the selected point  $(\boldsymbol{x},t)$  in the sweep event, plotted as functions of  $\delta s^+$ , calculated numerically with  $\Delta s = 10^{-3}$  and  $N = 10^7$ . The thin black lines are linear fits in semilogarithmic coordinates for  $\delta s^+ < -75$ .

the range  $\delta s^+ < -75$  in semilogarithmic coordinates are

$$\lambda_x^+ = 0.1039, \quad \lambda_y^+ = 0.1055, \quad \lambda_z^+ = 0.1069.$$
 (3.19)

These are about double the exponents reported in (3.18) for the ejection event. The greater size is reasonable, since in the sweep event the stochastic particles moving backward in time are lifted up by the flow higher into the buffer layer where local stretching

rates are largest (Johnson et al. 2017). Just as for the ejection considered previously, we conclude that the stochastic Cauchy vector at time s is exponentially stretched and rotated by transport from s to t, as pictured in the middle panel of Fig. 1. An important implication is that the constant mean of the stochastic Cauchy invariant demonstrated in Figs.2(a),4(a) is due to extensive cancellations of much larger magnitude vorticity vectors for individual realizations. We shall explore this finding further in paper II.

# 4. Conclusions and Prospects

We have explained the Constantin & Iyer (2008, 2011) theory for Navier-Stokes solutions as a stochastic Lagrangian representation in the Kuz'min (1983)-Oseledets (1989) formulation of the equation. The theory yields exact mean conservation laws for stochastic Cauchy invariants (in the generalized sense of Besse & Frisch (2017)) corresponding both to vortex-momentum and to vorticity. For wall-bounded flows, these conservation laws yield an exact representation of vorticity at any interior point as an average over stochastic vorticity contributions transported from the wall. We discussed some relations of the Constantin & Iyer (2008, 2011) results with the Eulerian theory of Lighthill (1963)-Morton (1984) for generation of vorticity at solid walls. We have also elaborated a numerical Monte Carlo method to calculate the stochastic Cauchy invariants and their statistics, given the Eulerian flow fields in space-time. These results hold for every Navier-Stokes solution, laminar as well as turbulent. We believe that the theory justifies stochastic Lagrangian flows as natural for viscous hydrodynamics, providing deeper analysis and insights into nonlinear vortex dynamics than the deterministic Lagrangian trajectories more suited to ideal fluids. In particular, the stochastic formulation fully represents the creation of vorticity at solid walls and its diffusion into the interior.

In the following paper II, we shall apply these exact mathematical and computational tools to investigate a concrete problem, the process of "lifting" of vortex lines from the wall into the buffer layer of turbulent channel flow. The present paper has validated the numerical Lagrangian scheme proposed in this work when used in conjunction with the simulation database for channel-flow turbulence documented by Graham et al. (2016). In particular, we have shown that the stochastic Cauchy invariant calculated by our methods has a well-conserved mean value, providing a stringent test on the fidelity of the numerical results to an exact Navier-Stokes solution. In the following paper, we shall explore the implications of the large cancellations in the conserved means of the stochastic Cauchy invariants which is implied by the exponential growth in their variances. We shall compare there our results and conclusions with those drawn from earlier experimental and computational studies. The long term goal of this line of research is to understand in detail the Lagrangian evolution of vorticity generated at the wall and to explicate the mechanisms by which a constant mean flux of spanwise vorticity is maintained.

An important related direction for future work is more efficient numerical methods. In this paper we have developed and applied the simplest Monte Carlo scheme with an Euler-Maruyama discretization of the equations of motion for stochastic Lagrangian particles. Unfortunately, the convergence rate in number of samples is quite slow, which significantly limits the range of applications. Within standard Monte Carlo, importance sampling techniques, e.g. by change of drift (Arouna 2004), can provide variance reduction and more efficient sampling of rare events. To get fundamental improvement of Monte Carlo rates of convergence, however, alternatives such as quasi-Monte Carlo (Hofmann & Mathé 1997) and multilevel Monte Carlo (Higham et al. 2013) should be explored. We believe that development of such improved numerical schemes is well worth the effort,

since stochastic Lagrangian analysis provides unique information on the flow physics not accessible by other means.

There are also clear directions for further work on mathematical and physical theory. As we shall discuss in Eyink et al. (2020b), the stochastic Lagrangian approach of Constantin & Iyer (2008, 2011) may be directly related to the Eulerian theory of Lighthill (1963)-Morton (1984) for vorticity generation at the wall. Closer ties should also exist with the Taylor (1932)-Huggins (1994) relation, which continues the mean vorticity flux into the interior of the flow. Our discussion in section 2.3 relates the stochastic Lagrangian trajectories to the Eulerian vorticity flux  $\Sigma$  integrated over any closed, bounded surface, but this result holds with any possible choice of flux. For example,  $\Sigma_{ij}^* := \epsilon_{ijk}\dot{u}_k$  is a perfectly acceptable definition of a "vorticity flux" which satisfies the balance equation (1.3), but its long-time average in the steady-state is zero! It should be possible to measure the distinguished flux (1.2) directly with stochastic trajectories, either pointwise or integrated over wall-parallel planes. If so, interesting physics questions could be addressed, such as how fresh vorticity injected at the wall is transported subsequently throughout the flow. Without a detailed proof, we note that an apparently natural measure of vorticity flux in terms of the stochastic Cauchy invariant can be calculated as

$$\lim_{s \to t-} \frac{1}{t-s} \mathbb{E}\left[ (\boldsymbol{x} - \widetilde{\boldsymbol{A}}_t^s(\boldsymbol{x})) \times \widetilde{\boldsymbol{\omega}}_s(\boldsymbol{x}, t) \right] = \boldsymbol{u}(\boldsymbol{x}, t) \times \boldsymbol{\omega}(\boldsymbol{x}, t) - 2\nu \nabla \times \boldsymbol{\omega}(\boldsymbol{x}, t). \tag{4.1}$$

The viscous contribution in (4.1) differs from that in the Eulerian flux (1.2) by a factor of 2, unfortunately, although this calculation does suffice to show that there must be organized vorticity transport by stochastic trajectories in the steady-state. Another theoretical topic deserving further work is the discrete approximation of continuous flows suggested by both Kuz'min (1983) and Oseledets (1989) in terms of N point-dipoles satisfying the Roberts (1972) equations. Fluid turbulence makes it natural to consider the statistical mechanics of such dipole systems. Just as with point-vortices, the regime of interest to statistical hydrodynamics is a non-extensive, high-energy limit with the flow volume fixed and the energy growing  $\propto N^2$  (Eyink & Spohn 1993). Finally, stochastic action principles analogous to that of Eyink (2010) can be investigated within the Kuz'min (1983)-Oseledets (1989) framework, especially for wall-bounded flows. It would be interesting to know in that case whether the conservation laws (2.52), (2.54) for stochastic Cauchy invariants can be derived as consequences of particle relabelling symmetry.

# Acknowledgements

We are grateful to Bérengère Dubrulle and Charles Meneveau for useful discussions and suggestions on this paper. We acknowledge the NSF grant BigData:OCE-1633124 for support and G.E. also acknowledges the Simons Foundation through Targeted Grant in MPS-663054 for partial support. This research project was conducted using simulation data from the Johns Hopkins Turbulence Database (JHTDB) and scientific computing services at the Maryland Advanced Research Computing Center (MARCC). Declaration of Interests: The authors report no conflict of interest.

### Appendix A. Stochastic Interpolation for Hitting Times & Locations

We consider first the stochastic interpolation for the hitting time  $\tilde{s}_*$  based upon the wall-normal coordinate  $\tilde{b}(s)$  of the stochastic particle. We suppose that the numerical integration has given  $\tilde{b}(s_i) = b_i$ , i = 0, 1 for times  $s_1 < s_0$  with  $|b_0| < h$  and  $|b_1| > h$ . For a particle hitting the wall at  $b = \pm h$ , the change of coordinates  $b \to b' = h \mp b$  transforms

the crossing into the event  $\tilde{b}'(s_0) = b_0' > 0$  and  $\tilde{b}'(s_1) = b_1' < 0$ . Hereafter we assume this transformation has been made and drop the primes. For small  $\Delta s = s_0 - s_1$ , the particle process can be written at times  $s \in (s_1, s_0)$  as

$$\tilde{b}(s) = b_0 + v(s - s_0) - \sqrt{2\nu} \,\tilde{W}_2(s),\tag{A 1}$$

where  $\tilde{W}_2(s)$  for  $s < s_0$  is a time-reversed Brownian motion with  $\tilde{W}_2(s_0) = 0$ . Imposing the conditions  $\tilde{b}(s_0) = b_0 > 0$  and  $\tilde{b}(s_1) = b_1 < 0$  then implies that  $\tilde{W}_2(s)$  is a generalized Brownian bridge satisfying for  $\Delta b := b_0 - b_1 > b_0 > 0$ 

$$\tilde{W}_2(s_0) = 0 < \frac{b_0}{\sqrt{2\nu}}, \quad \tilde{W}_2(s_1) = \frac{\Delta b - v\Delta s}{\sqrt{2\nu}} > \frac{b_0 - v\Delta s}{\sqrt{2\nu}}.$$
 (A 2)

The first hitting time  $\tilde{s}_* \in (s_1, s_0)$  when  $\tilde{b}(\tilde{s}_*) = 0$  then corresponds to the largest crossing time of the straight line  $b = (b_0 + v(s - s_0))/\sqrt{2\nu}$  and the Brownian bridge  $\tilde{W}_2(s)$ , or

$$\tilde{W}_2(s) = \frac{b_0 + v(s - s_0)}{\sqrt{2\nu}} \tag{A 3}$$

Determining this hitting time  $\tilde{s}_*$  can be mapped, by a sequence of transformations, onto a solved problem of determining the first hitting time of a standard Brownian motion with a straight line. First,  $\tilde{W}_2(s)$  can be related to a standard Brownian bridge  $\tilde{B}_2^{(0)}(s)$ , satisfying

$$\tilde{B}_2^{(0)}(s_0) = 0, \quad \tilde{B}_2^{(0)}(s_1) = 0,$$
 (A4)

by the transformation

$$\tilde{W}_2(s) = \left[ \frac{\Delta y - v\Delta s}{\sqrt{2\nu}} \right] \frac{s - s_0}{s_1 - s_0} + \tilde{B}_2^{(0)}(s). \tag{A5}$$

See Borodin & Salminen (2015), Part I, Chapter IV.4.21 (p.64, final statement). The first hitting time  $\tilde{s}_*$  is then determined as the largest time s such that

$$\tilde{B}_2^{(0)}(s) = \frac{1}{\sqrt{2\nu}} \frac{b_0(s_1 - s) + b_1(s - s_0)}{s_1 - s_0}.$$
(A6)

Next, the standard Brownian bridge  $\tilde{B}_{2}^{(0)}(s)$  can be mapped onto a standard Brownian motion  $\tilde{B}_{2}(\sigma)$  via the transformation

$$\tilde{B}_{2}^{(0)}(s) = \frac{s_{1} - s}{\sqrt{\Delta s}} \tilde{B}_{2} \left( \frac{s - s_{0}}{s_{1} - s} \right) \tag{A 7}$$

with the non-negative, dimensionless time variable  $\sigma:=\frac{s-s_0}{s_1-s}\in[0,\infty)$ . See Borodin & Salminen (2015), Part I, Chapter IV.4.21(b) (p.64). The first-hitting time is then given by the inverse formula  $\tilde{s}_*=\frac{s_0+\tilde{\sigma}_*s_1}{1+\tilde{\sigma}_*}$ , where  $\tilde{\sigma}_*$  is the smallest time  $\sigma$  such that

$$\tilde{B}_2(\sigma) = \frac{b_0 + b_1 \sigma}{\sqrt{2\nu \Lambda_s}} = \alpha - \beta \sigma, \qquad \alpha = \frac{b_0}{\sqrt{2\nu \Lambda_s}}, \quad \beta = \frac{|b_1|}{\sqrt{2\nu \Lambda_s}}$$
 (A8)

Equivalently,  $\tilde{s}_* = s_0 - \Delta \tilde{s}_*$  with  $\Delta \tilde{s}_* = \Delta s \frac{\tilde{\sigma}_*}{1 + \tilde{\sigma}_*}$ .

The statistical distribution of the first-hitting time  $\tilde{\sigma}_*$  of a standard Brownian motion  $\tilde{B}_2(\sigma)$  and the straight line  $\alpha - \beta \sigma$  is well-known to have the form

$$p(\sigma) = \frac{|\alpha|}{\sqrt{2\pi\sigma^3}} \exp\left(-\frac{(\alpha - \beta\sigma)^2}{2\sigma}\right) = \left(\frac{\lambda}{2\pi\sigma^3}\right)^{1/2} \exp\left(-\frac{\lambda(\sigma - \mu)^2}{2\mu^2\sigma}\right) \tag{A 9}$$

with parameters

$$\lambda = \alpha^2 = \frac{b_0^2}{2\nu\Delta s}, \quad \mu = \frac{\alpha}{\beta} = \left|\frac{b_0}{b_1}\right|.$$
 (A 10)

See Borodin & Salminen (2015), Part II, formula 2.02 (p.295). In the second form, this probability density is known as the *inverse Gaussian distribution*  $IG(\mu, \lambda)$  with parameters  $\mu$ ,  $\lambda$  (Chhikara & Folks 1988). A simple algorithm was devised by Michael *et al.* (1976) to obtain realizations  $\tilde{\sigma}_*$  drawn from the distribution  $IG(\mu, \lambda)$ , by a transformation of a normal random variable  $\tilde{N}$ . One first constructs a chi-square random variable

$$\tilde{\chi} = \mu \tilde{N}^2 \tag{A 11}$$

and then sets

$$\tilde{\xi} = 1 + \left(\tilde{\chi} - \sqrt{4\lambda\tilde{\chi} + \tilde{\chi}^2}\right)/2\lambda.$$
 (A 12)

Finally, with probability  $1/(1+\tilde{\xi})$  one selects  $\tilde{\sigma}_* = \mu \tilde{\xi}$  and otherwise selects  $\tilde{\sigma}_* = \mu/\tilde{\xi}$ . Below is a snippet of a Fortran code which implements this algorithm:

```
n1=normal
chi=mu*n1**2
xi=chi-sqrt(abs(4*lambda*chi+chi**2))
xi=1+xi/(2*lambda)
u1=uniform
if (u1 .le. 1/(1+xi)) then
  sigma=mu*xi
else
  sigma=mu/xi
end if
```

For constant wall-normal velocity v the above algorithm is exact with no constraint on the size of  $\Delta s$  and it gives a statistically correct sampling of  $\tilde{\sigma}_*$  and  $\tilde{s}_* = \frac{s_0 + \tilde{\sigma}_* s_1}{1 + \tilde{\sigma}_*}$ . In an incompressible fluid flow the wall-normal velocity decreases to zero quadratically with the distance to the wall, so the algorithm should again provide an excellent approximation.

Streamwise and spanwise locations of the stochastic Lagrangian particle at the first hitting time  $\tilde{s}_*$  can be obtained in a statistically accurate fashion by a similar approach. For example, suppose that the streamwise position at the two integration times takes on the values  $\tilde{a}(s_0) = a_0$ ,  $\tilde{a}(s_1) = a_1$ . Between them it is accurately represented for small  $\Delta s$  by the equation

$$\tilde{a}(s) = a_0 + u(s - s_0) + \sqrt{2\nu} \,\tilde{W}_1(s),$$
(A 13)

with  $\tilde{W}_1(s)$  for  $s < s_0$  another time-reversed Brownian motion satisfying  $\tilde{W}_1(s_0) = 0$ . Imposing the second end-point condition on  $\tilde{a}(s_1)$  then implies that  $\tilde{W}_1(s)$  becomes a generalized Brownian bridge satisfying

$$\tilde{W}_1(s_0) = 0, \quad \tilde{W}_1(s_1) = \frac{\Delta a - u\Delta s}{\sqrt{2\nu}}.$$
 (A 14)

We now make the same transformations as before, namely:

$$\tilde{W}_1(s) = \left(\frac{\Delta a - u\Delta s}{\sqrt{2\nu}}\right) \frac{s - s_0}{s_1 - s_0} + \tilde{B}_1^{(0)}(s) \tag{A15}$$

for a standard Brownian bridge  $\tilde{B}_{1}^{(0)}(s)$  and

$$\tilde{B}_1^{(0)}(s) = \frac{s_1 - s}{\sqrt{\Delta s}} \tilde{B}_1(\sigma) = \frac{\sqrt{\Delta s}}{1 + \sigma} \tilde{B}_1(\sigma) \tag{A 16}$$

for a standard Brownian motion  $\tilde{B}_1(\sigma)$  with  $\sigma = \frac{s-s_0}{s_1-s}$ . Together these give

$$\tilde{a}(s) = \frac{a_0(s_1 - s) + a_1(s - s_0)}{s_1 - s_0} + \frac{\sqrt{2\nu\Delta s}}{1 + \sigma}\tilde{B}_1(\sigma),\tag{A 17}$$

which is linear interpolation with a stochastic correction. In particular, the streamwise location at the time  $\tilde{s}_*$  of first hitting of the wall is

$$\tilde{a}_* := \tilde{a}(\tilde{s}_*) = \frac{a_0(s_1 - \tilde{s}_*) + a_1(\tilde{s}_* - s_0)}{s_1 - s_0} + \frac{\sqrt{2\nu\Delta s}}{1 + \tilde{\sigma}_*} \tilde{B}_1(\tilde{\sigma}_*). \tag{A 18}$$

Likewise, the spanwise location is

$$\tilde{c}_* := \tilde{c}(\tilde{s}_*) = \frac{c_0(s_1 - \tilde{s}_*) + c_1(\tilde{s}_* - s_0)}{s_1 - s_0} + \frac{\sqrt{2\nu\Delta s}}{1 + \tilde{\sigma}_*} \tilde{B}_3(\tilde{\sigma}_*). \tag{A 19}$$

The two new Brownian motions at the single time  $\tilde{\sigma}_*$  are statistically represented by  $\tilde{B}_i(\tilde{\sigma}_*) = \sqrt{\tilde{\sigma}_*}\tilde{N}_i$ , i = 1, 3 where  $\tilde{N}_1$ ,  $\tilde{N}_3$  are new independent normal random variables.

#### REFERENCES

Anderson, P. W. 1966 Considerations on the flow of superfluid helium. Reviews of Modern Physics 38 (2), 298.

Arnold, V. 1966 Sur la géométrie différentielle des groupes de Lie de dimension infinie et ses applications à l'hydrodynamique des fluides parfaits. Annales de l'institut Fourier 16 (1), 319–361

Arouna, Bouhari 2004 Adaptative monte carlo method, a variance reduction technique. *Monte Carlo Methods and Applications* **10** (1), 1–24.

Batchelor, G.K. 2000 An Introduction to Fluid Dynamics. Cambridge University Press.

Berrut, Jean-Paul & Trefethen, Lloyd N 2004 Barycentric lagrange interpolation. SIAM review 46 (3), 501–517.

Besse, N. & Frisch, U. 2017 Geometric formulation of the Cauchy invariants for incompressible Euler flow in flat and curved spaces. *Journal of Fluid Mechanics* 825, 412–478.

BORODIN, A. N. & SALMINEN, P. 2015 Handbook of Brownian Motion - Facts and Formulae. Birkhäuser Basel.

Box, G. E. P. & Muller, M. E. 1958 A note on the generation of random normal deviates. The Annals of Mathematical Statistics 29 (2), 610–611.

BOYER, F. & FABRIE, P. 2012 Mathematical Tools for the Study of the Incompressible Navier-Stokes Equations and Related Models. Springer, New York.

Brenier, Yann 2003 Topics on hydrodynamics and volume preserving maps. In *Handbook of mathematical fluid dynamics* (ed. S. Friedlander & D. Serre), , vol. 2, pp. 55–86. Elsevier.

Brown, Garry L & Roshko, Anatol 2012 Turbulent shear layers and wakes. Journal of Turbulence  ${\bf 13},~{\rm N51}.$ 

CAUCHY, A. L. 1815 Sur l'état du fluide à une époque quelconque du mouvement. Mémoires extraits des recueils de l'Académie des sciences de l'Institut de France, Théorie de la propagation des ondes à la surface d'un fluide pesant d'une profondeur indéfinie. (Extraits des Mémoires présentés par divers savants à lAcadémie royale des Sciences de l'Institut de France et imprimés par son ordre). Sciences mathématiques et physiques. Tome I, 1827 Seconde Partie, pp. 33–73.

Chhikara, R. & Folks, J. L. 1988 The Inverse Gaussian Distribution: Theory: Methodology, and Applications. Taylor & Francis.

Constantin, P. & Iyer, G. 2008 A stochastic Lagrangian representation of the 3-dimensional incompressible Navier-Stokes equations. *Commun. Pure Appl. Math.* **61**, 330–345.

Constantin, P. & Iyer, G. 2011 A stochastic-Lagrangian approach to the Navier-Stokes equations in domains with boundary. *The Annals of Applied Probability* **21.4**, 1466–1492.

DRIVAS, THEODORE D & EYINK, GREGORY L 2017 A lagrangian fluctuation—dissipation relation for scalar turbulence. part ii. wall-bounded flows. *Journal of Fluid Mechanics* 829, 236–279.

- EYINK, GL & SPOHN, H 1993 Negative-temperature states and large-scale, long-lived vortices in two-dimensional turbulence. *Journal of statistical physics* **70** (3-4), 833–886.
- EYINK, G. L. 2008 Turbulent flow in pipes and channels as cross-stream inverse cascades of vorticity. *Physics of Fluids* **20** (12), 125101.
- EYINK, G. L. 2010 Stochastic least-action principle for the incompressible Navier-Stokes equation. Physica D: Nonlinear Phenomena 239 (14), 1236-1240.
- EYINK, G. L., GUPTA, A., WANG, M. & ZAKI, T. A. 2019 SCauchy A Fortran90 code to calculate stochastic Cauchy invariants. https://github.com/mzwang2012/SCauchy.git.
- EYINK, G. L., GUPTA, A. & ZAKI, T. A. 2020a Near-wall vorticity dynamics in channel-flow turbulence: A stochastic Lagrangian analysis. J. Fluid Mech. (submitted), https://arxiv.org/abs/1912.06684.
- EYINK, G. L., ZAKI, T. A. & WANG, M. 2020b A stochastic Lagrangian representation of the Lighthill-Morton theory. in preparation.
- Falkovich, G, Gawdzki, K & Vergassola, Massimo 2001 Particles and fields in fluid turbulence. Reviews of modern Physics 73 (4), 913.
- FREIDLIN, M. I. 1985 Functional Integration and Partial Differential Equations. Princeton University Press.
- FRIEDMAN, A. 2006 Stochastic Differential Equations and Applications. Mineola, NY: Dover.
- FRISCH, U. & VILLONE, B. 2014 Cauchy's almost forgotten Lagrangian formulation of the Euler equation for 3D incompressible flow. *The European Physical Journal H* **39** (3), 325–351.
- Graham, J., Kanov, K., Yang, X. I. A., Lee, M., Malaya, N., Lalescu, C. C., Burns, R., Eyink, G., Szalay, A., Moser, R. D. & Meneveau, C. 2016 A web services accessible database of turbulent channel flow and its use for testing a new integral wall model for Les. *Journal of Turbulence* 17 (2), 181–215.
- Guala, M., Liberzon, A., Lüthi, B., Kinzelbach, W. & Tsinober, A. 2006 Stretching and tilting of material lines in turbulence: the effect of strain and vorticity. *Physical Review E* 73 (3), 036303.
- Guala, M., Lüthi, B., Liberzon, A., Tsinober, A. & Kinzelbach, W. 2005 On the evolution of material lines and vorticity in homogeneous turbulence. *Journal of Fluid Mechanics* 533, 339–359.
- HELMHOLTZ, H. VON 1858 Über Integrale der hydrodynamischen Gleichungen welche den Wirbelbewegungen entsprechen. Journal für die reine und angewandte Mathematik 55, 25–55.
- HIGHAM, DESMOND J, MAO, XUERONG, ROJ, MIKOLAJ, SONG, QINGSHUO & YIN, GEORGE 2013 Mean exit times and the multilevel monte carlo method. SIAM/ASA Journal on Uncertainty Quantification 1 (1), 2–18.
- HOFMANN, NORBERT & MATHÉ, PETER 1997 On quasi-monte carlo simulation of stochastic differential equations. *Mathematics of Computation* **66** (218), 573–589.
- Huggins, E. R. 1970 Energy-dissipation theorem and detailed Josephson equation for ideal incompressible fluids. *Physical Review A* 1 (2), 332.
- Huggins, E. R. 1994 Vortex currents in turbulent superfluid and classical fluid channel flow, the Magnus effect, and Goldstone boson fields. *Journal of low temperature physics* 96 (5-6), 317–346.
- IYER, GAUTAM 2006 A stochastic Lagrangian formulation of the incompressible Navier-Stokes and related transport equations. PhD thesis, The University of Chicago, Department of Mathematics, Chicago, IL.
- Johnson, P. L., Hamilton, S. S., Burns, R. & Meneveau, C. 2017 Analysis of geometrical and statistical features of lagrangian stretching in turbulent channel flow using a database task-parallel particle tracking algorithm. *Physical Review Fluids* 2 (1), 014605.
- Johnson, P. L. & Meneveau, C. 2016 Large-deviation statistics of vorticity stretching in isotropic turbulence. *Physical Review E* **93** (3), 033118.
- Josephson, B. D. 1962 Possible new effects in superconductive tunnelling. *Physics letters* 1 (7), 251–253.
- Keanini, RG 2006 Random walk methods for scalar transport problems subject to dirichlet, neumann and mixed boundary conditions. *Proceedings of the Royal Society A: Mathematical, Physical and Engineering Sciences* **463** (2078), 435–460.

- KELVIN, L. 1868 VI.-On vortex motion. Transactions of the Royal Society of Edinburgh 25 (1), 217–260.
- KIM, J., MOIN, P. & MOSER, R. 1987 Turbulence statistics in fully developed channel flow at low Reynolds number. *Journal of fluid mechanics* 177, 133–166.
- Kloeden, P. E. & Platen, E. 2013 Numerical solution of stochastic differential equations, , vol. 23. Springer Science & Business Media.
- KOUMOUTSAKOS, P. 1999 Vorticity flux control for a turbulent channel flow. *Physics of Fluids* 11 (2), 248–250.
- KUNITA, H. 1997 Stochastic Flows and Stochastic Differential Equations, Cambridge Studies in Advanced Mathematics, vol. 24. Cambridge, UK: Cambridge Univ. Press.
- Kuz'min, G. A. 1983 Ideal incompressible hydrodynamics in terms of the vortex momentum density. Physics Letters A 96 (2), 88–90.
- LEE, M., MALAYA, N. & MOSER, R. D. 2013 Petascale direct numerical simulation of turbulent channel flow on up to 786K cores. In SC '13, Proceedings of the International Conference on High Performance Computing, Networking, Storage and Analysis, Denver, Colorado November 17 - 21, 2013, Article 61. ACM, New York.
- LI, Y., PERLMAN, E., WAN, M., YANG, Y., MENEVEAU, C., BURNS, R., CHEN, S., SZALAY, A. & EYINK, G. 2008 A public turbulence database cluster and applications to study Lagrangian evolution of velocity increments in turbulence. *Journal of Turbulence* 9, N31.
- LIGHTHILL, M. J. 1963 Boundary layer theory. In *Laminar Boundary Layers* (ed. L. Rosenhead), pp. 46–113. Oxford University Press, Oxford.
- LÜTHI, B., TSINOBER, A. & KINZELBACH, W. 2005 Lagrangian measurement of vorticity dynamics in turbulent flow. *Journal of Fluid mechanics* **528**, 87–118.
- Lyman, FA 1990 Vorticity production at a solid boundary. Appl. Mech. Rev 43 (8), 157–158.
- $\label{lem:matsumoto} \begin{tabular}{lll} Matsumoto, & M. & 1997-present & . & Mersenne & Twister & Home & Page. & http://www.math.sci.html. \\ & hiroshima-u.ac.jp/~m-mat/MT/emt.html. \\ \end{tabular}$
- MATSUMOTO, M. & NISHIMURA, T. 1998 Mersenne twister: a 623-dimensionally equidistributed uniform pseudo-random number generator. ACM Transactions on Modeling and Computer Simulation (TOMACS) 8 (1), 3–30.
- MICHAEL, J. R., SCHUCANY, W. R. & HAAS, R. W. 1976 Generating random variates using transformations with multiple roots. *The American Statistician* **30** (2), 88–90.
- MORTON, B. R. 1984 The generation and decay of vorticity. Geophysical & Astrophysical Fluid Dynamics 28 (3-4), 277–308.
- Oksendal, Bernt 2013 Stochastic differential equations: an introduction with applications. Springer Science & Business Media.
- ORSZAG, S. A. 1971 On the elimination of aliasing in finite-difference schemes by filtering high-wavenumber components. *Journal of the Atmospheric sciences* **28** (6), 1074–1074.
- OSELEDETS, V. I. 1989 On a new way of writing the Navier-Stokes equation. The Hamiltonian formalism. Russian Mathematical Surveys 44 (3), 210.
- PACKARD, R. E. 1998 The role of the Josephson-Anderson equation in superfluid helium. Reviews of Modern Physics 70 (2), 641.
- Panton, R.L. 1984 Incompressible Flow. John Wiley & Sons.
- RAPOPORT, DIEGO L 2002 Random diffeomorphisms and integration of the classical Navier-Stokes equations. Reports on Mathematical Physics 49 (1), 1–27.
- REZAKHANLOU, F. 2016 Stochastically symplectic maps and their applications to the Navier–Stokes equation. Annales de l'Institut Henri Poincare (C) Non Linear Analysis 33 (1), 1–22.
- ROBERTS, P. H. 1972 A Hamiltonian theory for weakly interacting vortices. *Mathematika* **19** (2), 169–179.
- Salmon, R. 1988 Hamiltonian fluid mechanics. Annual review of fluid mechanics 20 (1), 225–256.
- Sawford, Brian 2001 Turbulent relative dispersion. Annual review of fluid mechanics 33 (1), 289–317.
- Shraiman, Boris I & Siggia, Eric D 1994 Lagrangian path integrals and fluctuations in random flow. Physical Review E  $\bf 49$  (4), 2912.
- TAYLOR, G. I. 1932 The transport of vorticity and heat through fluids in turbulent motion.

- Proceedings of the Royal Society of London. Series A, Containing Papers of a Mathematical and Physical Character 135 (828), 685–702.
- Taylor, G. I. 1937 The statistical theory of isotropic turbulence. *Journal of the Aeronautical Sciences* 4 (8), 311–315.
- TAYLOR, G. I. 1938 Production and dissipation of vorticity in a turbulent fluid. Proceedings of the Royal Society of London. Series A-Mathematical and Physical Sciences 164 (916), 15–23.
- Taylor, G. I. & Green, A. E. 1937 Mechanism of the production of small eddies from large ones. Proceedings of the Royal Society of London. Series A-Mathematical and Physical Sciences 158 (895), 499–521.
- Tur, A. V. & Yanovsky, V. V. 1993 Invariants in dissipationless hydrodynamic media. *Journal of Fluid Mechanics* **248**, 67–106.
- VAROQUAUX, ERIC 2015 Anderson's considerations on the flow of superfluid helium: Some offshoots. Reviews of Modern Physics 87 (3), 803.
- WEBER, H. 1868 Über eine Transformation der hydrodynamischen Gleichungen. Journal für die reine und angewandte Mathematik 68, 286–292.
- Wu, J-Z. & Wu, J-M. 1993 Interactions between a solid surface and a viscous compressible flow field. *Journal of Fluid Mechanics* **254**, 183–211.
- Wu, J-Z. & Wu, J-M. 1996 Vorticity dynamics on boundaries. Advances in applied mechanics 32, 119–275.
- Wu, J-Z. & Wu, J-M. 1998 Boundary vorticity dynamics since Lighthill's 1963 article: review and development. *Theoretical and computational fluid dynamics* **10** (1-4), 459–474.
- Zhao, H., Wu, J.-Z. & Luo, J.-S. 2004 Turbulent drag reduction by traveling wave of flexible wall. Fluid Dynamics Research 34 (3), 175.